Cortical drive and thalamic feed-forward inhibition control thalamic output synchrony during absence seizures

Cian Mccafferty, Francois David, Marcello Venzi, Magor L Lőrincz, Francis
Delicata, Zoe Atherton, Gregorio Recchia, Gergely Orban, Régis Lambert,
Giuseppe Di Giovanni, et al.

Cortical drive and thalamic feed-forward inhibition control thalamic output synchrony during absence seizures

Cian McCafferty[#,1,2,*], **François David**[#,1,3], **Marcello Venzi**[1], **Magor L. Lőrincz**[4], **Francis Delicata**[1,5], **Zoe Atherton**[1], **Gregorio Recchia**[1], **Gergely Orban**[1,5], **Régis C. Lambert**[6], **Giuseppe Di Giovanni**[1,5], **Nathalie Leresche**[6], and **Vincenzo Crunelli**[1,5,*]

[1]Neuroscience Division, School of Bioscience, Cardiff University, Museum Avenue, Cardiff CF10 3AX, UK

[2]Department of Neurology, Yale University School of Medicine, New Haven, Connecticut 06520, USA

[3]Team Waking, Lyon Neuroscience Research Center, CRNL, INSERM U1028, CNRS UMR5292, University of Lyon 1, Lyon, France

[4]Department of Physiology, Anatomy and Neuroscience, University of Szeged, Szeged, Hungary

[5]Department of Physiology and Biochemistry, University of Malta, Msida, Malta

[6]Sorbonne Université, CNRS, Inserm, Neuroscience Paris Seine - Institut de Biologie Paris Seine (NPS - IBPS), F-75005 Paris, France

[#] These authors contributed equally to this work.

Abstract

Behaviorally and pathologically relevant cortico-thalamo-cortical oscillations are driven by diverse interacting cell-intrinsic and synaptic processes. However, the mechanism that gives rise to the paroxysmal oscillations of absence seizures (ASs) remains unknown. Here we report that during ASs in behaving animals, cortico-thalamic excitation drives thalamic firing by preferentially eliciting tonic rather than T-type Ca^{2+} channels (T-channels)-dependent burst firing in thalamocortical (TC) neurons, and by temporally framing thalamic output via feed-forward reticular thalamic (NRT)-to-TC neuron inhibition. In TC neurons, overall ictal firing is markedly reduced and bursts rarely occur. Moreover, block of T-channels in cortical and NRT neurons suppresses ASs, but in TC neurons has no effect on seizures or on ictal thalamic output synchrony. These results demonstrate ictal bidirectional cortico-thalamic communications and provide the

first mechanistic understanding of cortico-thalamo-cortical network firing dynamics during ASs in behaving animals.

Introduction

Cortico-thalamo-cortical circuits process behaviourally relevant internal and external information, determine vigilance states, and elicit diverse forms of neuronal network oscillations during sleep[1–3]. Reciprocal excitation between neocortex and thalamus allows the synchronization of these brain regions, while cortico-thalamic afferents also excite GABAergic nucleus reticularis thalami (NRT) neurons, thus driving feed-forward inhibition of thalamocortical (TC) neurons[4]. Inhibition of TC neurons can evoke a rebound T-type Ca^{2+} channel (T-channel)-mediated burst of action potentials that in turn excites cortical targets, as well as NRT neurons leading to intrathalamic feed-back inhibition[4]. This thalamic rhythmogenesis contributes to or determines many physiological cortico-thalamo-cortical oscillations[5], in particular those underlying spindle, slow-wave and delta oscillations of non-REM sleep that require T-channel bursts in both TC and NRT neurons[1,5,6].

The T-channel bursts of these thalamic neuronal populations are also considered essential for the thalamic rhythmogenesis of typical absence seizures (ASs), a type of non-convulsive seizure characterized by sudden loss of consciousness and spike-wave-discharges (SWDs) in the EEG[7–9]. Indeed, currently accepted AS mechanisms, supported by *in vitro*[10,11] and *in silico*[12,13] studies, require the presence of bursts in both TC and NRT neurons at each SWD cycle, with $GABA_A$/$GABA_B$ receptors and intrinsic Ca^{2+}-/Na^+-activated K^+ currents contributing to the rhythmicity of these neuronal populations, respectively. However, these studies are limited by the compromised network integrity and absence of behavioural correlates inherent to *in vitro* preparations. In contrast, studies that examined the activity of thalamic neurons in intact animals under fentanyl or anesthesia report either a paucity of T-channel bursts in TC neurons[14] or the presence of two populations of TC neurons, one almost fully silent and the other with occasional bursts intermixed with single action potentials[15], whereas NRT neurons show bursts at each SWD cycle[15,16]. The relevance of these, and other *in vivo* investigations using multi-unit activity[17], is also limited given the lack of behavioural seizures and the profound effects of fentanyl and anesthesia on SWD properties[18,19]. Thus, we still have no knowledge of the TC and NRT neuron firing dynamics and interactions during behavioral ASs.

Here, using ensemble recordings of single somatotopically-aligned thalamic and cortical neurons during genetically-determined or pharmacologically-induced ASs in freely moving rats, we found complex temporal dynamics of TC and NRT neuron firing, with TC neurons exhibiting a marked decrease in overall firing and a paucity of burst firing. Selective block of T-channels in NRT and cortical neurons decreased ASs, whereas their block in TC neurons did not affect seizure expression. Cortical excitatory and NRT inhibitory input to

TC neurons during seizures, as well as cortical excitation of NRT neurons, suggest a role for ictal feed-forward inhibition of TC neurons. Taken together, these results demonstrate that during behavioural ASs the synchronous, seizure-perpetuating output of TC neurons is not determined by the dynamics of their T-channel-mediated burst firing but rather is driven by top-down cortical excitation and sharpened by cortically driven, T-channel-dependent NRT inhibition.

Results

Ensemble recordings of single thalamic neurons during ASs

Using microdrive-mounted silicon probes (Supplementary Fig. 1d), alone or with microdialysis probe(s)20, we studied under freely moving conditions the interictal (between seizures) and ictal (during seizures) firing dynamics of TC neurons of the ventrobasal thalamic nucleus (VB) and NRT neurons in two well-established AS models: the Genetic Absence Epilepsy Rats from Strasbourg (GAERS)19 and the pharmacological γ-hydroxybutyrate (GHB) model21 (Online Methods). The VB was chosen because the somatosensory system has a crucial role in ASs of these models where SWDs originate from a cortical initiation site, the peri-oral region of primary somatosensory cortex (S1pO)22,23, before spreading to the VB and then to other cortical regions (Supplementary Fig. 2). Individual action potential waveforms were isolated from the full-band raw signal, semi-automatically clustered following systematic visual inspection24 (Fig. 1) (Supplementary Fig. 1a) and classified as originating from excitatory (i.e. TC) or inhibitory (i.e. NRT) neurons based on standard criteria25 (Fig. 1b-d). Reliable identification of thalamic T-channel bursts during ASs was demonstrated by i) the agreement of burst signatures (Fig. 1c) and action potential waveforms (Fig. 1d) with those currently used in TC and NRT neuron classification25, and ii) the similarity of burst features of each isolated neuron during periods of varying synchrony, i.e. seizures and sleep (compare Fig. 1c and Supplementary Fig. 1e) (Supplementary Fig. 3d) (Online Methods).

TC neuron ictal activity

We recorded 139 TC neurons in 6 GAERS during 4,214 ASs (duration: 11.5±4.4 s, mean ±SEM) with a SWD frequency of 7.1±0.5 Hz. Single TC neurons were markedly less active (52%) ictally than interictally (5.44±0.03 vs 11.4±0.04 Hz, p<0.001) (Fig. 2a-c) (Supplementary Table 1), an effect driven by a reduction in tonic firing (2.8±0.01 vs 9.3±0.03 Hz, p<0.001) (Fig. 2e) and a large incidence of electrical silence: 45% of TC neurons (62 out of 139) were silent for >50% of spike-and-wave complexes (SWCs), the individual cycles of SWDs (Fig. 3a). The decrease of total and tonic firing started 2 s before SWD detection in the EEG (Fig. 2c,e). By contrast, the interictal rate (0.40±0.01 Hz) of T-channel bursts started to increase rapidly 1 s before seizure onset, peaked (1.8±0.22 Hz) just after seizure onset (400 ms) and then decayed within the next 2 s to a stable level (0.9±0.01 Hz, p<0.05 compared to interictal) for the remainder of a seizure (Fig. 2d,f-h). Thus, the ictal incidence of bursts was low (15.7±0.1% of SWCs) (Fig. 3b,e) while tonic firing occurred during 30.1±0.1% of SWCs (Fig. 3c,f), leading to a total firing rate of 0.85±0.01 spikes/SWC (Fig. 3d). Notably, despite the scarce ictal firing of individual TC neurons, there was a strong and rhythmic ictal thalamic output as indicated by the cross-correlograms

(XCors) of simultaneously recorded TC neurons (Supplementary Fig. 4a). Moreover, the absolute and relative rates of tonic and burst firing of individual TC neurons could greatly vary between seizures (Supplementary Fig. 5).

In summary, the firing of single TC neurons during ASs in behaving GAERS is characterized by i) multi-staged temporal dynamics, ii) a marked decrease in total and tonic firing, and iii) an increase in burst rate, though bursts only occur at every 7th SWC.

NRT neuron ictal activity

Two classes of NRT neurons could be identified on the basis of their firing during awake/interictal periods[26]: wake-active (WA, >10 Hz) and wake-quiescent (WQ, ≤10 Hz) (Supplementary Fig. 1b). The total firing (47±1.8 Hz) of WA NRT neurons (n=13) in GAERS started to decrease 3 s prior to SWD detection, reached a minimum of 31±0.9 Hz (500 ms prior to SWD detection) (p<0.01), and then, in contrast to TC neurons, sharply increased to a peak of 62.1±0.2 Hz (p<0.01) at interictal-to-ictal transition (Fig. 2c,i,j) (Supplementary Table 1). Then, it slowly decreased to a stable ictal level of 52±2 Hz (p<0.05 compared to interictal) (Fig. 2c). In contrast, tonic firing (25±1 Hz) started to decrease 3 s prior to SWD detection, reaching a stable value of 14±2 Hz (p<0.001) (Fig. 2e). This decrease in WA NRT neuron tonic firing was overcompensated for by an enhancement of burst firing, which started to increase (from 0.31±0.01 Hz interictally) at the same time as TC neuron bursts, peaked (2.4±0.02 Hz, p<0.05) about 2.5 s after seizure onset and then slowly decreased for the remainder of a seizure (1.4±0.03 Hz at ictal-to-interictal transition) (Fig. 2d,i-j). Although bursts in WA NRT neurons occurred on average during 25±2% of SWCs, a group of neurons showed bursts in about 50% of SWCs and another group in <1% (Fig. 3g). Tonic firing was present during 53±2.5% of SWCs, and the ictal total firing of WA NRT neurons was 6.2±0.3 spikes/SWC (Fig. 3g,h).

Since WQ NRT neurons (n=12) did not show any significant AS-associated variation in firing (Fig. 2), or any significant AS-linked feature in subsequent analyses (Supplementary Fig. 6), they will not be discussed hereafter, and WA NRT neurons will be referred to as NRT neurons.

In summary, the firing of GAERS NRT neurons during ASs exhibit i) multi-staged temporal dynamics, and ii) increased total and burst firing rates. However, in individual NRT neurons bursts do not occur at every SWC.

Synchrony and coherence of ictal thalamic neuron firing

Having characterized the firing dynamics of individual thalamic neurons during ASs, we investigated the synchrony and communication strength between TC and NRT neuronal ensembles. SWC-spike-triggered averages indicated that GAERS TC and NRT neuron total firing peaked 15 ms before and 9 ms after the SWC-spike, respectively (Fig. 4a) (Supplementary Table 2), though the initial ascending phase of the two population curves showed a strong overlap. Burst and tonic firing peaks had similar shape and latency (to the SWC-spike) to those of total firing (Fig. 4a).

However, SWC-spike-triggered averages are affected by the coherence and the amount of neuronal firing, an issue of critical importance here in view of the marked firing differences between the two thalamic populations. Interestingly, cumulative distribution functions of peak firing times relative to the SWC-spike, which are unaffected by these properties, were similar for TC and NRT neurons (Fig. 4b) (p=0.631; Kolmogorov-Smirnov test). This suggests that the TC and NRT populations are excited by a common source.

To understand interactions between the firing mode and the EEG paroxysmal oscillation, we analysed the coherence of TC and NRT neuron firing with the SWC-spike. TC neurons whose total firing peak was just before the SWC-spike (-20 to 0 ms) were highly coherent compared to those whose peak was outside this window (Fig. 4c). In contrast, NRT neurons with a firing peak before the SWC-spike showed very low coherence whereas those that preferentially fired after the SWC-spike had high coherence (Fig. 4c). Moreover, TC neuron coherence was little influenced by firing type (Fig. 4e), whereas NRT neurons showed significantly higher coherence (p<0.001) when they fired bursts (Fig. 4f). Consistently, NRT neurons with more overall burst firing were more coherent with respect to the SWC-spike (Fig. 4d), whereas for TC neurons a high burst rate was not necessary for high coherence (not shown).

In summary, GAERS TC and NRT neurons show synchronous activation with respect to the SWC-spike. Furthermore, whereas NRT burst firing is more coherent than tonic, TC neurons have similar coherence for both firing types, suggesting that TC neuron bursts are not essential for paroxysmal synchrony.

Recruitment of intrathalamic inhibition

The paucity of TC neuron bursts, the high coherence of their tonic firing with SWDs, and the overlap of TC and NRT cumulative firing probabilities challenge the view that TC neuron bursts are necessary to drive cortical and NRT populations during seizure[10,11,13]. Thus, it was important to investigate the synaptic interactions between the two thalamic neuronal populations during ASs. XCors of the ictal firing of simultaneously recorded TC and NRT neuron pairs (n=14) had broad peaks, often before time-zero (Fig. 5a, Supplementary Fig. 6a), indicating an increased probability of NRT neurons to fire after TC neurons. Those peaks were absent during interictal periods (Fig. 5f) and reduced during non-REM sleep (Fig. 5g).

Thirty-six percent (5 out of 14) of GAERS TC-NRT pairs showed a significant post-zero trough indicating a decreased TC neuron firing probability following an NRT action potential (Fig. 5a), and thus an ictally active NRT-TC inhibitory connection. These inhibitory patterns were still present in XCors between TC neuron total firing and NRT neuron bursts (Fig. 5b), but were absent in XCors calculated using NRT neuron tonic firing (Fig. 5d), demonstrating that the decreased firing probability of TC neurons depends on NRT neuron bursts[10]. In contrast, the troughs were still present when TC neuron tonic firing was used for the XCors, indicating that TC neuron bursts are not required for these ictal intrathalamic interactions (Fig. 5c). Notably, NRT neurons that had relatively flat autocorrelograms showed neither significant peaks nor troughs in their XCors with TC neurons (Supplementary Fig. 6a-e).

In summary, ASs involve intrathalamic inhibition via the recruitment of NRT-TC neuron inhibitory assemblies, which are dependent on NRT but not TC neuron burst firing.

TC and NRT neurons of the GHB model had similar ictal firing dynamics, distributions and XCors to GAERS (Supplementary Figs. 7 and 8; Supplementary Tables 1 and 2).

Cortico-thalamo-cortical drive and feed-forward inhibition

The lack of evidence for a TC neuron burst-dependent excitatory drive of NRT neurons (Fig. 5e), together with the similar ictal firing distributions of TC and NRT neurons (Fig. 4b), suggests that the corticofugal input may be a key source of excitation of both thalamic neuron populations, thus leading to intrathalamic feed-forward inhibition. To directly investigate this possibility, we next simultaneously recorded thalamic and somatotopically aligned (Online Methods) putative pyramidal neurons in the S1pO cortical region of 3 GAERS (see Supplementary Fig. 9 for cortical neuron isolation and classification). Multiple pairs (13/58) of TC and cortical excitatory neurons showed two peaks in their ictal total firing XCors, suggesting bidirectional excitation (Fig. 6a). XCors that only included cortical burst firing (Fig. 6a) had a larger post-zero peak compared to those of tonic (Supplementary Fig. 10a) and total firing (Fig. 6a), indicating enhanced cortical to TC neuron excitation when cortical neurons fired bursts. Conversely, TC burst firing XCors had almost no post-zero component (Fig. 6a), indicating that cortical excitation selectively drives TC neuron tonic firing. Moreover, XCors associated with the largest SWC-spikes (i.e. 4th quartile of amplitude) showed enhanced TC-cortex and cortex-TC excitation compared to those with smaller SWC-spikes (i.e. 1st quartile) (Fig. 6d,e) (Supplementary Fig. 10b), indicating that TC and cortical neurons are more effectively recruited during cycles with higher cortical synchrony. Notably, the gain in strength of the cortex-TC interactions was higher than that of TC-cortex interactions (Fig. 6f), indicating that increased SWC-spike amplitude is accompanied by enhanced cortical (over thalamic) influence on network dynamics.

XCors of pairs of simultaneously recorded NRT and cortical neurons had only post-zero peaks for any type of firing, indicating a clear excitatory drive from cortical to NRT neurons, which was strongest when cortical neurons fired bursts (Fig. 6b) and elicited both tonic and burst firing in NRT neurons (Fig. 6b; Supplementary Fig. 10c). Notably, the probability of NRT neuron firing was higher in the 10 ms periods after a cortical than a TC neuron action potential, indicating that the cortex is a more significant source of ictal NRT excitation (Fig. 6c).

In summary, during ASs i) bi-directional excitation occur between cortical and TC neuron populations, ii) cortical drive preferentially elicits tonic and not burst firing in TC neurons, and iii) cortical firing is evoked by both tonic and burst firing of TC neurons. Finally, the presence of stronger excitatory drive from cortex to NRT neurons than from TC to NRT neurons suggests that the intra-thalamic inhibition recruited ictally (Fig. 5a-c) most likely represents a cortex-dependent feed-forward mechanism.

TC neuron T-channels do not contribute to ictal thalamic output synchrony

Since the above results do not support a thalamo-cortical pacemaker mechanism involving TC neuron T-channel-mediated burst firing[7,10,11,13], we directly tested the contribution of

these channels to the ictal TC neuron output. T-channels were blocked by administration of the selective antagonist TTA-P2[27] via reverse microdialysis *unilaterally* into the VB of freely behaving GAERS while simultaneously recording single TC neuron activity from an adjacent silicone probe. TTA-P2 (300 μM in the inlet dialysis probe) abolished high-frequency bursts in all recorded TC neurons (n=7) during ASs as well as sleep, but tonic firing persisted during ASs and wakefulness, though reduced by 57±6% and 33±3% of pre-drug rates (p<0.01 and p<0.05, respectively) (Fig. 7a,b). Significantly, following TTA-P2-elicited block of bursts, TC neuron total and tonic firing distributions expressed peaks with similar strength of phase preference and time relative to the SWC-spike as before antagonist application (Kuiper test, n=7, p>0.05) (Fig. 7c,d).

These data demonstrate that TC neurons are capable of delivering strong synchronous output to the neocortex during ASs even when their T-channels (and burst firing) are fully blocked and, notably, that these channels are not required for dictating the ictal firing time of TC neurons.

Cortical and NRT but not TC neuron T-channels are essential for ASs

Though the above results indicate that TC neuron T-channels are not necessary for the synchronized ictal thalamic output to neocortex, they do not obviate a critical role for these channels in ASs. Thus, we next applied TTA-P2 *bilaterally* by reverse microdialysis in freely moving GAERS using a method that had established the spatio-temporal profile of TTA-P2-mediated full block of thalamic T-channels[28] (Online Methods). Specifically, our microdialysis dose-response and time-response analyses (see Fig. 3 in Ref. 28) showed that TTA-P2 applied at a concentration of 300 μM from a probe positioned in the center of the VB abolishes (in ~ 20 minutes) T-channel bursts within a volume that entirely encompasses this thalamic nucleus without affecting NRT neuron T-channels. Blocking T-channels throughout the VB with 300 μM TTA-P2 in 8 GAERS using the above protocol did not affect ASs (Fig. 7e,f) (Supplementary Fig. 11). In contrast, extending the block of T-channels to the NRT in 6 other GAERS by increasing TTA-P2 concentration (and thus affected tissue volume[28]) to 1 mM decreased ASs (Fig. 7e,f). Since in the latter experiment TTA-P2 would have also spread medially to the posterior nucleus, we then administered 300 μM TTA-P2 750 μm laterally from the centre of the VB in 6 other GAERS, thus affecting the NRT and avoiding the posterior nucleus. In this case too, the number and total duration of ASs were decreased by 50% (Fig. 7e,f) (Supplementary Fig. 11). In a different group of GAERS (n=9) we inserted the probe 750 μm more medially from the centre of the VB, thus fully avoiding the spread of TTA-P2 into the NRT. In this case, 1 mM TTA-P2 had no effect on ASs (Fig. 7e,f) (Supplementary Fig. 11).

Recent studies showing that brain-wide genetic knock-out or enhancement of CaV3.1 channels (the main T-channel subtype present in TC neurons[29]) abolishes[30] or induces[31] ASs, respectively, have been interpreted as suggesting a necessary role of TC neuron T-channels. Since CaV3.1 channels are also heavily expressed in neocortex[29], we tested the effect on ASs of their antagonism by TTA-P2 in the latter region. TTA-P2 (1 mM) applied by bilateral microdialysis in the S1pO (i.e. the initiation site of genetic rat SWDs[22,23]) of 16 GAERS decreased ASs by 36% (Fig. 7b) (Supplementary Fig. 11).

Together with T-channel-mediated burst firing, GABA$_B$ receptors of TC neurons were suggested to be a key determinant of the temporal dynamics of TC neuron firing that underlie ictal thalamic rhythmogenesis and determine SWD frequency[10,12,13]. Thus, we next investigated the effect of bilateral microdialysis (in the centre of the VB) of the GABA$_B$ antagonist CGP55845 at sub-maximal concentration (500 μM). This drug markedly suppressed the total time spent in ASs (aCSF: 87.0±18.3%; CGP55845: 5.69±1.4% of control, n=10 GAERS, p = 0.0156, Wilcoxon paired signed-rank two-sided test), as previously shown for other GABA$_B$ antagonists[8,19], but had no effect on the frequency of the SWDs of the remaining seizures (aCSF: 6.88±0.1 Hz; CGP55845: 6.74±0.1 Hz, p=0.5781, n=7, Wilcoxon paired signed-rank two-sided test).

In summary, these results demonstrate that T-channels of NRT and cortical, but not TC, neurons are necessary for the expression of behavioural ASs.

Top-down excitation enables ictal TC neuron recruitment in the absence of burst firing

To test the neuronal mechanism of thalamic firing during ASs suggested by the experimental results, we used a simple biophysical network model (Fig. 8a) (Online Methods) (Supplementary Table 3). It includes one TC neuron that is connected only via GABA$_A$ synapses to two NRT neurons, one that preferentially fires bursts and one that has both tonic and burst firing (cf. Fig. 3g) due to a more depolarized membrane potential (Fig. 8a,b). Two cortical pyramidal neurons are connected to the NRT neurons, and reciprocally to the TC neuron, via AMPA synapses (Fig. 8a). Simulations were driven by trains of 5 EPSPs delivered only to the cortical neurons at 7 Hz (Fig. 8a,b), i.e. the frequency of GAERS SWDs[19].

The model (Supplementary Fig. 12a) reproduced the TC and NRT neuron firing distributions observed experimentally (Fig. 4a). Notably, the firing peak of the more depolarized NRT neuron occurred earlier than that of the NRT neuron that preferentially fired bursts (Supplementary Fig. 12a), and was coincident with the TC neuron peak firing when NRT-TC synapses were blocked (Supplementary Fig. 12c). Moreover, increasing the strength of TC-NRT synapses (up to 6-fold higher than the CX-NRT synapses) did not affect the firing distribution (Supplementary Fig. 12b). By contrast, removing cortical-to-NRT synapses (Supplementary Fig. 12f) or T-channels in NRT neurons (Supplementary Fig. 12h) resulted in deviation of the distributions from both the simulated control conditions (Supplementary Fig. 12a) and the experimental results (Fig. 4a). Furthermore, removing inhibitory NRT-to-TC synapses significantly broadened the peak of the TC firing distribution (k=2.03 vs k=3.59, p<0.001; Kuiper test) (Supplementary Fig.12c), supporting the sharpening effect of NRT inhibition on thalamic output.

XCors of the simulated firing closely reproduced those observed experimentally, notably in the presence of a trough in TC-NRT XCors (compare Fig. 8c and 5a) and in the occurrence of two peaks in the TC-CX XCors (compare Fig. 8c and 6a). Similar to the simulated firing distributions, the various XCors were not qualitatively affected by a large increase in TC-to-NRT synapse strength (compare Fig. 8c and d) or removal of TC T-channels (Fig. 8i). As expected, removing TC-to-CX (Fig. 8f) or CX-to-TC (Fig. 8g) synapses abolished the peak before or after time-zero, respectively. Removing NRT-to-TC inhibition (Fig. 8e), CX-NRT

excitation (Fig. 8h), or NRT T-channels (Fig. 8j) also generated XCors lacking key features of simulated control conditions and experimental results: the post-zero trough in TC-NRT, the post-zero peak in NRT-CX, and the narrow peaks in all XCors, respectively.

In summary, these simulations confirm that i) fast GABA$_A$-mediated NRT-to-TC inhibition is sufficient to sharpen TC neuron ictal firing, ii) a strong TC-to-NRT excitatory connection is not required to explain the ictal firing of NRT neurons, and iii) bidirectional excitation between TC and cortical neurons coupled with cortical drive of NRT neurons can explain the experimentally observed ictal interactions between the two thalamic neuronal populations and among cortical and thalamic neuronal assemblies.

Discussion

Neuronal ensemble activity of single thalamic and cortical neurons demonstrates synchronous bidirectional cortico-thalamo-cortical communication during ASs in behaving animals. The cortical and NRT components of this activity are T-channel-dependent, and required for AS expression. The TC neuron population contributes synchronous volleys of, mainly tonic, firing that are driven by cortical excitation and framed by, mainly feed-forward, NRT-mediated inhibition.

Thalamic firing dynamics

The disagreements between our findings and previous studies indicate that the use of brain slices[10,11] or anesthetized/fentanyl conditions[14–16,23] result in different TC and NRT neuron ictal firing dynamics than those of behavioural ASs. Specifically, our results show that during ASs, total firing of TC neurons is markedly decreased as well as temporally framed within each SWD cycle, and that the synchrony and strength of TC ictal output to the neocortex is not a feature of single, rhythmically bursting TC neurons but is an emergent property of this population, as suggested originally by Buzsaki[32]. This contrasts with the conclusions of a recent study[33], in which behavioural ASs were induced and suppressed by switching TC firing between a rhythmic and non-rhythmic mode, respectively, with the former mode's synchrony being indirectly attributed to T-channel-dependent bursts on the basis of *in vitro* optogenetic experiments. Although the significance of thalamic synchrony to ASs is not contradicted by our present work, the cellular or synaptic cause of that synchrony would not have been detectable at the level of multi-unit activity used by Sorokin et al.[33]. Furthermore, even if one were to assume that TC neuron T-channel-dependent bursts were responsible for that study's induction of ASs, this does not imply that they are an inevitable and necessary component of the paroxysmal oscillation. In fact, when single-cell resolution is achieved, as in our current work, ictal thalamic output synchrony is shown to be reliant not upon T-channels, but rather upon excitation and feed-forward inhibition of cortical origin.

The ictal reduction of total firing in TC neurons of both GAERS and GHB models may result from their increased tonic GABA$_A$ inhibition[34,35]. Such increased tonic GABA$_A$ inhibition has also been shown to prolong the decay of GABA$_A$ IPSPs evoked in TC neurons by NRT neuron single action potentials or bursts[36], which could explain the ability

of NRT burst-induced IPSPs to completely suppress TC output through most of the SWD cycle.

Considering that tonic inhibition provides 90% of GABA$_A$ inhibition in TC neurons[37], the gain-of-function of TC neuron extrasynaptic GABA$_A$ receptors in epileptic animals[34] is sufficient to explain the electrical silence, the marked decrease of tonic firing and the paucity of rebound bursts observed ictally in GAERS TC neurons. This, in turn, may provide the thalamic basis for the decreased response to sensory stimulation during ASs[8,9].

The peak in TC neuron burst firing at the start of ASs may result from the time-dependent plasticity that is known to occur at both excitatory cortical-TC and inhibitory NRT-TC synapses: optogenetic stimulation of cortico-thalamic afferents at 10 Hz (a frequency similar to rodent SWDs) initially evokes in VB TC neurons a synaptic sequence of a small inward-large outward current, which transforms into a stable large inward-small outward current within the first second of stimulation[38].

Role for T-channels

Our findings question the view that TC neuron burst firing is critical for ASs[7,10,12,13]. First, the unaltered synchrony of ictal thalamic output to the neocortex during a block of TC burst firing demonstrates that these channels do not determine SWD frequency, as was previously proposed[7,10,11]. The lack of effect on SWD frequency of blocking GABA$_B$ receptors in TC neurons further contradicts the mechanistic hypothesis in which synaptic GABA$_B$ receptor current and cell-intrinsic T-channel current interact to determine the timing of TC neuron firing and, thus, SWD frequency[10,12,13]. The partial block of thalamic tonic firing output by TTA-P2 may be explained by the small but significant contribution of T-channels to tonic firing and the input-output function of TC neurons at depolarized membrane potentials because of the physiologically significant fraction of T-channels that are de-inactivated at these potentials[39]. However, we cannot exclude that some single spikes included in our tonic firing classification may be generated by a low-threshold spike.

Second, the lack of effect on ASs of TTA-P2 applied in the VB demonstrates that T-channels of this nucleus, somatotopic to the cortical initiation site[22,23], are not required for the expression and maintenance of these seizures. By contrast, sleep spindles, a cortico-thalamo-cortical network oscillation with a well-established thalamic rhythmogenesis[5,6], are abolished when T-channels of VB TC neurons are blocked by an identical TTA-P2 microdialysis application[28] as in the current work.

Notably, the reduction in ASs following the block of T-channels in cortical neurons indicates that bursts in the neocortex (and possibly other regions, that could include non-sensory thalamic nuclei) underlie the effects on ASs following brain-wide genetic manipulations of CaV3.1 channels[30,31]. Meanwhile, the marked reduction in ASs following the block of NRT neuron T-channels confirm that CaV3.2 and/or CaV3.3 channels, the two T-channel subtypes present in these neurons[29], play a key role in genetically determined ASs, as indicated by CaV3.2 channel mutations in GAERS NRT neurons[40] and human absence epilepsy cohorts[41]. Notably, however, GHB-induced ASs are resistant to the knockout of both CaV3.2 and CaV3.3 channels[42].

Ictal cortico-thalamo-cortical interactions

Our results provide direct evidence that NRT-TC inhibitory short-term assemblies become engaged ictally in a manner that is critically dependent on NRT bursts and fast $GABA_A$ synapses. This is indicated by the lack of NRT-TC inhibition in XCors that considered only NRT neuron tonic firing, and the close similarity between experimental XCors of TC and NRT neuron ictal firing and those simulated using only $GABA_A$ synapses. Thus, fast NRT inhibition frames ictal TC neuron firing, and the higher coherence of NRT neuron burst firing that occurs just after the SWC-spike is likely to reflect sharpening of the TC neuron response by these bursts.

The lack of a sharp peak in TC-NRT neuron XCors does not suggest an ictal, strongly active monosynaptic connection between TC and NRT neuron pairs, and modelled ictal firing and interactions were not altered by varying TC-NRT synapse strength. This absence of a major involvement of TC-NRT excitatory synapses during ictal firing interactions may be an unexpected finding since this connection has been reported to be strong and reliable in juvenile rats43. However, in adult animals tonic TC neuron firing at 40 Hz evokes only small EPSPs in NRT neurons, whereas TC bursts evoke larger NRT EPSPs (Fig. 9 in Ref. 44). In view of this, and of our observed ictal 6 Hz tonic and 1 Hz burst ictal firing rates, relatively weak (but not absent) ictal TC-NRT compared to cortex-NRT excitation is not surprising. Indeed, optogenetic stimulation of cortico-thalamic afferents is not highly effectively in activating the TC-to-NRT pathway *in vitro*45, supporting the lower probability of ictal NRT firing following TC than cortical neuron firing that we observed.

In summary, our findings show that ASs do not rely on widespread TC neuron bursts but rather cortico-thalamic inputs exciting both TC and NRT neurons, and thalamic feed-forward inhibition. Thus, the most parsimonious mechanism of a SWD cycle involves reciprocal excitation of TC and cortical neurons, as well as excitation of NRT neurons mainly by cortico-thalamic neurons. The precise timing of this excitation may depend on intra-cortical rhythmogenic mechanisms as well as cortico-thalamic interactions. NRT neuron firing then temporally frames TC neuron output by suppressing firing throughout most of the spike-wave cycle. The framed TC output may help to re-engage, and synchronize, the cortex in the next cycle, but rebound bursts are not a necessary part of this output, contrasting with thalamic slice and *in silico* models7,10–13. In other words, the temporal precision of TC neuron ictal firing is not dictated by the interaction of T-channel activation/inactivation and $GABA_A$/$GABA_B$ IPSP dynamics10,12,13 but rather by the interplay of excitatory cortico-thalamic and fast feed-forward NRT inhibitory drives, which are known to shape cortico-thalamo-cortical activity in other behavioural contexts38,45,46. On the other hand, the interplay of cortico-thalamic input and cell-intrinsic mechanisms (including T-current and Ca^{2+}-activated currents9) underlie NRT neuron ictal excitation.

Significance for human ASs

The strong similarities in firing dynamics and neuronal interactions of ASs between a polygenic (GAERS) and a pharmacological (GHB) model suggest that similar mechanisms may underlie generalized non-convulsive seizures in other models with spontaneous or induced single-gene mutations47. Nevertheless, selective impairment of cortex-to-NRT

transmission, leading to a reduction of feed-forward inhibition of TC neurons, can induce ASs48, and it would be of interest to investigate the ictal mechanism of human R43Q knock-in mice that, in contrast to the GAERS and GHB models, have decreased tonic $GABA_A$ inhibition in TC neurons49. These different models undoubtedly offer useful insights on the mechanisms underlying the large diversity in SWD waveform and AS severity encountered in childhood and juvenile absence epilepsy patient50.

Online Methods

Experiments were approved under the UK Animals (Scientific Procedures) Act 1986 by Cardiff University Animal Welfare and Ethics Committee and were conducted in accordance with current recommendations for experimental work in epilepsy51. All data will be made available on reasonable request by contacting one of the corresponding authors. Further details of experimental design, software, materials, reagents, animal research participants, and data availability can be found in the Life Sciences Reporting Summary.

No statistical methods were used to pre-determine sample sizes, but our sample sizes are similar to those reported in previous publications25,34. In the case of bilateral microdialysis experiments, animals were randomly assigned to receive drug or control first. Experimenters were blind to the group of animals when detecting time spent in seizure. Animals were excluded from microdialysis experiments only in the case of visible distress, and neurons were excluded from ensemble recording experiments if the reconstructed electrode position lay outside the VB/NRT.

Surgery and implantation

Male GAERS and Wistar rats (both 4-7 month old), with access to food/water *ad libitum*, were maintained on a 12:12 hour light:dark cycle (light on at 08:00 am). Surgery anesthesia was maintained with isoflurane and body temperature with a homoeothermic heat blanket. EEG gold-plated screws (Svenska Dentorama, UK) were implanted in fronto-parietal sites.

For ensemble unit recordings, four-shank, linear, 32-site silicon probes (Buzsaki32L, NeuroNexus, Michigan, USA) were immersed in detergent at 60°C for 2-4 hours, before being rinsed with deionized water and immersed in Vybrant Dil dye (Invitrogen) solution prior to insertion (Supplementary Fig. 1c). Each silicon probe was lowered into the VB (AP: -3.35 mm, ML: 2.9 mm)52, such that its lower end rested 4mm ventral from the brain surface, i.e. at the top of the VB. A microdrive was then secured with grip cement that was also used to create a mini-Faraday cage and protective structure of copper mesh53. When an additional silicon probe was implanted in S1pO cortex, its coordinates were AP: - 0.0 mm, ML: 5.5 mm) and its tip was initially positioned in cortical layer 2/3.

For experiments with bilateral microdialysis, two guide cannulae for CMA 12 microdialysis probes (Linton Instruments, UK) were lowered into the centre of the VB (VB (c) in Fig. 7b), such that their tips rested at AP: -3.35 mm, ML: 2.8 mm, DV: -4.4 mm. To target the NRT, probes were positioned adjacent to but not within the NRT so to avoid excessive damage of this narrow nucleus (AP: -3.2 mm, ML: 3.5 mm, DV: -4.2 mm). The coordinates for the probes positioned more medially than the centre of the VB (VB (m) in Fig. 7b) were AP:

-3.35 mm, ML: 2.1 mm, DV: -4.4 mm, and those targeting S1pO cortex were AP: -3.2 mm, ML: 5.5 mm, DV: -0.5 mm.

Simultaneous unilateral implantation of a silicon probe and a microdialysis cannula was similar to the one described above, with the microdialysis cannula being lowered into the brain at a 16° angle with respect to the vertical axis in the rostro-caudal plane such that its tip rested close to the silicon probe (AP -3.5 mm, ML 2.8 mm, DV -6 mm20.

All electrical and microdialysis components were affixed to the skull with methylacrylic cement, and the final cap structure incorporated all electrode wires and microdialysis guide cannulae. Rats were allowed to recover for ≥5 days.

Behavioral experiments

For all behavioral experiments, each animal was placed individually in a purpose-built plexiglass box housed within a Faraday cage. Animals were continuously monitored throughout a procedure by an experimenter and by video recordings (using Spike2 video software, CED, Cambridge, UK) to precisely time-match EEG and neuronal ensemble recordings with behavior (see below). A counterweighted swivel arm positioned above the recording box allowed free movement of the animal while connected to electrical and microdialysis equipment.

Neuronal ensemble recordings—The head-mounted Plexon HST/32V-G20 VLSI-based preamplifier was connected to a Plexon data acquisition system (sampling rate: 20 kHz). Online filtering was used to visualize the raw signal as either LFP (low-pass filter at 300 Hz) or as spiking/unit activity (high-pass filter at 500 Hz). Upon connection to the recording apparatus, the presence or absence (on any channels) of neurons suitable for recording was assessed based on the shape and amplitude of any visible spikes. If no such neurons were present after 30 minutes of observation, the silicon probe was lowered deeper into the brain by turning the microdrive, while recording the number and degree of turns of the microdrive screw to allow post-hoc reconstruction of the recording site (see below). A similar procedure was used for simultaneous recordings of thalamic and cortical neurons.

For GAERS, each recording session lasted no more than 3 hours depending on the quality and stability of the recorded neurons and the behavior of the animal during the session. In the GHB model (100 mg/kg i.p. of γ-butyrolactone, a GHB pro-drug), recordings were limited by the time course of the drug (about 1 hour). GAERS sessions included multiple bouts of non-REM sleep, which were used to characterize the properties of the T-channel mediated high-frequency bursts of each recorded thalamic neuron for subsequent comparison with the high-frequency bursts recorded from the same neuron during multiple ASs (see below).

Bilateral reverse microdialysis—Dummy probes within the guide cannulae were replaced with CMA 12 microdialysis probes (Linton Instruments, UK) 18 hours prior to the start of a recording session. For GAERS, each experiment involved 1 hour habituation of the animal to the recording environment after the inlet tubes of the microdialysis probes had been connected (via FEP tubing, 0.18 μL/cm internal volume, Linton Instruments, UK) to a

1 mL syringe placed in a 4-channel microdialysis pump (CMA 400, Linton Instruments, UK). The second hour consisted of EEG recording during reverse microdialysis of artificial cerebrospinal fluid (aCSF) at a rate of 1 μL/min. At the end of the second hour, either reverse microdialysis of aCSF was continued or a solution containing TTA-P2 (300 μM or 1 mM) or CGP-55845 (500 μM) was administered via different syringes for an additional 80 min.

A minimum delay of 6 days occurred between subsequent experiments to allow wash-out of the drug. Each animal was only recorded twice, once with aCSF and once with TTA-P2 administration, and was randomly allocated to receive first aCSF or TTA-P2. The effect of TTA-P2 was quantified during the 40-80 min period ("treatment hour") (Fig. 7e) from the start of its microdialysis since our previous experiments under similar conditions had shown that 20 min are necessary to achieve a steady block of TC neuron burst firing throughout the required extent of the VB (see ref. 37 for additional information). Effects of microdialysis-applied TTA-P2 on ASs are reported as percentage of the aCSF treatment (Fig. 7e,f).

Simultaneous neuronal ensemble recordings and unilateral reverse microdialysis—Silicon electrodes were employed as described earlier for neuronal ensemble recordings. Microdialysis probe cannulae were inserted as described above under surgical procedures, in order that the membrane of the microdialysis probe would extend beneath the VB thalamus, allowing the silicon electrode to be moved gradually towards the membrane by microdrive adjustment[20]. Upon identification of suitable and stable neurons, a recording control period was carried out before 300 μM TTA-P2 was administered. Neuronal firing dynamics were investigated as described below for the periods before and after full block of bursts by TTA-P2 had been detected.

Data analysis

AS detection and SWDs analysis—The EEG was recorded using an SBA4-v6 BioAmp amplifier (SuperTech Inc., Hungary), digitized at 1 kHz (by a Cambridge Electronic Design, CED, Micro3 D.130) and analyzed with CED Spike2 v7.3 and Matlab (R2011b, The Mathworks Inc., USA). SWDs were identified using the SeizureDetect script (Spike2, CED, Cambridge, UK). Firstly, baseline EEG (desynchronized, active or resting wakefulness) was identified manually and voltage amplitude thresholds set at 5-7 standard deviations (SD) above or below the mean. Secondly, the following parameters for initial event detection were applied to all points that crossed this threshold (crossings): maximum time between initial two crossings of 0.2 s, maximum time between any two crossings within an event of 0.35 s, minimum of 5 crossings per event, minimum time of 0.5 s between any two events for them to count as separate (otherwise overriding 0.35 s limit and merging events), and a minimum event duration of 1 s. The final component of the SeizureDetect script gated detected events by dominant frequency band (calculated by time intervals between crossings rather than by spectrographic analysis). Events with >75% of intervals within the 5-12 Hz range were classified as SWDs. Designated SWDs were then visually inspected to ensure the above parameters and the signal-to-noise ratio were appropriate for effective identification and isolation. All EEG sections identified as SWDs were then crossed-checked with the corresponding video recordings: those that showed the concurrent presence

of behavioral arrest were then classified as ASs, while the very few that did not were excluded from further analysis.

Behavioral state classification—EEG recordings were divided into one of three behavioral states: non-REM sleep, wakefulness, and ASs. Isolation of ASs (i.e. concomitant presence of behavioral arrest and SWDs in the EEG) was carried out as detailed above. Detection of non-REM sleep periods, from the sections of the EEG and video recordings that did not contain ASs, was achieved by plotting cumulative power over the 0.5 to 4 Hz frequency range of the EEG signal, and setting a threshold at 2.5 SD above the baseline value during a visually identified period of wakefulness, and post-hoc analysis of the video recordings. The remaining time (i.e. neither ASs or non-REM sleep) was classified as wakefulness upon confirmation of a desynchronized (low amplitude, high frequency) EEG. Note that ASs only developed during wakefulness, and thus the pre-ictal periods used for the analysis of interictal-to-ictal transitions only included wakefulness. Periods of non-REM sleep were extremely rare in GHB injected Wistar rats due to the relatively short duration (about 1 hour) of the recording period.

Action potential sorting—Extraction of action potentials was performed with different subroutines[20,24]. The signal was high-pass filtered and thresholded to extract action potential shapes (Fig. 1b) (Supplementary Fig.1a), using the first 3 principal components of each action potential on each channel (8 channels per group for the Buzsaki32L probe) as features. The first stage of clustering used the unsupervised KlustaKwik program[54] to group action potentials with similar features into clusters based on a Classification Expectation Maximization (CEM) algorithm[55–59] (Fig. 1a). The second stage involved supervised refinement of appropriate clusters and elimination of unsuitable clusters. Action potential waveforms were constant and distinct during non-REM sleep and wakefulness but some would at times be insufficiently large, relative to the high frequency multi-unit noise observed at each SWC cycle, to sort during ASs. In this case the entire cluster was eliminated.

Neuron and firing pattern classifications—Thalamic neurons

Isolated action potentials recorded from locations outside the VB/NRT region were excluded for further analysis. The remaining action potentials were classified as TC or (fibers belonging to) NRT neurons[25] on the basis of i) the properties of their T-channel dependent high frequency bursts during non-REM sleep (Supplementary Fig. 1e), ii) the action potential half-width (Fig. 1d) and iii) the ratio of the first to the shortest interspike interval (ISI) (Fig. 1d). A high frequency burst was defined as three or more spikes with an ISI of ≤ 7 ms that were preceded by a silent interval of ≥100 ms. NRT neurons were classified as those with an acceleration index (ratio of first to shortest ISIs in a burst) greater than 1.4, while TC neurons have a ratio < 1.3 (Refs. 60,61) (Fig. 1d). Moreover, NRT neurons tended to exhibit a smaller spike half-width than TC neurons (Fig. 1d). These properties are in agreement with the previously reported "accelerando-decelerando" pattern of NRT bursts[60,61] (Fig. 1c2) (Supplementary Fig. 1d) and the sharper waveform of the action potentials of inhibitory compared to excitatory neurons[25,62] (Fig. 1d, inset).

Total firing reported in the text and figures for both types of thalamic neurons includes all sorted spikes, while tonic firing includes all spikes separated by two ISI > 7 ms in order to discard spike potentially belonging to bursts. Action potential doublets which did not fall into the tonic firing classification were post-hoc included in all burst firing calculation because of the marked similarity of their temporal dynamics before, during and after ASs with bursts of ≥ 3 action potentials (Supplementary Fig. 1e). A proportion of spikes could not be conclusively classified as being either burst or tonic firing, and amounted to the following percentages: GAERS TC neurons: $10.0 \pm 8.9\%$, wake-active NRT neurons: $4.1 \pm 0.8\%$, wake-quiescent NRT neurons: $2.4 \pm 1.5\%$; GHB TC neurons: $2.48 \pm 2.27\%$, wake-active NRT neurons: $9.7 \pm 3.5\%$, wake-quiescent NRT neurons: $3.7 \pm 0.4\%$. These spikes, however, were all included in the total firing.

Burst, tonic and total firing rates in each of the three behavioral conditions, as well as during transitions between conditions, were calculated across entire recording sessions (Supplementary Table 1). Transitions from wakefulness to seizure and vice versa were investigated by plotting mean activity rates (± SEM) 5 s before and after seizure start and end times, respectively. Only seizures of ≥ 5 s (for GAERS) or ≥ 2 s (for GHB) duration with preceding/following (as appropriate) wake periods of at least the same length were selected.

Cortical neurons

Isolated cortical neurons were classified as putative excitatory cells and distinguished from putative inhibitory cells on the basis of their trough-to-peak times and spike half-widths62 (Supplementary Fig. 9). Functional somatotopic alignement of the thalamic and cortical regions were verified by sending brief air puffs to the perioral zone of the GAERS rats. The majority of neurons in both brain regions responded within 10 ms to this sensory stimulation.

Neuron-neuron and neuron-EEG relationships

These were investigated during each behavioral state, with neuron-SWC relationships also studied during ASs. Auto- and cross-correlograms (XCors) were calculated using the xcorr function of Matlab in 1-ms bins. SWC spike-triggered EEG averages were calculated by taking mean values of ictal total, tonic and burst rates (burst time taken as time of first spike in a burst) across entire recording sessions, and then averaging across all neurons of the same type (TC, WA NRT, WQ NRT). SWC spike-triggered firing averages used SWC spike as reference. This involved finding all local amplitude maxima more than 3 SD above the mean EEG amplitude and then selecting the largest of these maxima within each SWC. Spike and burst rates were averaged in 1 ms bins around these peaks. Other measures that quantified activity relative to the SWC required definition of SWC epochs. These were extrapolated from spike peak detections by selecting periods between adjacent peaks with intervals less than 300 ms. These epochs were used to calculate per-SWC total firing, tonic firing and bursts across entire recording sessions.

Coherence—Total firing, burst firing and tonic firing distribution were selected between -70 and +70ms around the SWC spike time and normalized to get the density distribution binned per ms. Vectors were then circularized by linearly converting the -70 to +70 ms interval into an angle from $-\pi$ to π. The module of the average vector computed over all density values at each angle bin was then estimated in the complex domain to give the coherence. This measure is comparable to a spike-field coherence[63].

SWC-spike amplitude—The amplitude of the SWC-spikes was measured from the EEG recordings. Neuronal spikes used for cross-correlations based on SWC-spike amplitudes were extracted from periods around those SWCs of the smallest (1st) and largest (4th) quartiles (Fig. 6e,f, Supplementary Fig. 10b,c). Analysis of the XCorrs were done for pairs of neurons that had an amplitude 20ms around the time lag=0ms of at least 8 times the basal chance level found beyond 20ms away from the lag=0. This ensured that thalamic and cortical neurons fire in a correlated manner for the directional analysis. Twenty-four (out of 58) TC-cortical pairs satisfied this criterion. Then, peak ratios were measured as ratios between 1) the maximum amplitudes corresponding to time lags between -10ms and 0ms in the Xcors for the thalamo-cortical direction measurement and to time lags between 0 and 10ms in the XCors for the cortico-thalamic direction measurement for either the 1st or 4th quartile, and 2) the same measurement for all SWCs no matter their amplitude. Those values were then normalized per SWC. The resulting peak ratios indicate changes in the strengths of thalamo-cortical (TC) (Fig. 6d) and cortico-thalamic (CX) (Fig. 6e) interactions with respect to changes in the amplitude of the SWC-spike. Lastly, a ratio wascomputed between CX and TC unidirectional peak ratio (Fig. 6f).

Histological processing

For animals used in the microdialysis experiments, 1 μL of thionine dye was administered via both inlet and outlet channels of the microdialysis probes with stripped membranes using a 10 μL Hamilton syringe in order to highlight the probes' tracks. At the end of all experiments, animal received a lethal dose of Euthatal before being transcardially perfused with phosphate-buffered saline (PBS, 0.9% NaCl) followed by paraformaldehyde (PFA, buffered in 0.9% NaCl PBS). Microdialysis and/or silicon probes were then carefully withdrawn from the brain, which was then immersed in 4% PFA for 4 hours. Brains were refrigerated in 0.9% NaCl PBS until required. Brain sections around the region of interest were cut at a thickness of 100 μm on a Leica VT 1000S vibratome while immersed in chilled 0.9% NaCl PBS. For microdialysis experiments, slices were photographed using a Nikon D90 camera (Nikon Imaging, UK) and then inspected for actual site of recording. For neuronal ensemble recording experiments, slices were photographed under an Olympus BX61 microscope at 4x magnification in brightfield and with a TRITC filter. Images were merged using Adobe Photoshop (Supplementary Fig. 1c), and the final position of the electrode tip was marked. The position of the recording site during each session was then calculated from the noted microdrive movements.

Drugs

The aCSF for the microdialysis experiments was purchased from Tocris Biosciences (Bristol, UK). 3,5-dichloro-N-[1-(2,2-dimethyl-tetrahydro-pyran-4-ylmethyl)-4-fluoro-

piperidin-4-yl-methyl]-benzamide (TTA-P2) was a kind gift from Merck Inc. (USA). TTA-P2 was dissolved in DMSO (2% of final solution) before addition to aCSF. An identical concentration of DMSO was added to the aCSF solutions. (2*S*)-3-[[(1*S*)-1-(3,4-dichlorophenyl)ethyl]amino-2-hydroxypropyl] (phenylmethyl) phosphinic acid hydrochloride (CGP-55845) was purchased from Tocris (UK). The pH of all dialysis solutions was 7.

Simulations

Using Neuron software[64], a previously developed[39] single compartment conductance model of a TC neuron was connected to two NRT neuron models[65] and to two cortical pyramidal neuron (PY) models[66], which were also connected to the TC neuron and the two NRT neurons (Fig. 8a) (see Supplementary Table 3 for network description and synapse properties). T-type Ca^{2+} channels had a conductance of 40 nS and a reversal potential of 120 mV in TC neurons. The two NRT neurons received a different constant current injection in order to set their membrane potential in a different range, thus favoring (NRT2) or not (NRT1) the emergence of T-channel bursts. Single AMPA synapses from TC to NRT neurons and single $GABA_A$ synapses from NRT to the TC neuron were similar to those described in Ref. 65. AMPA synapses from TC to CX, from CX to TC, and from CX to NRT were modelled as single exponential conductances (ExpSyn object in Neuron with a decay time constant of 2 ms), with a transmission delay of 2 ms to represent inter-area communications. Their synaptic weights were either 0, when connections were inactive, or as reported in Supplementary Table 3. All neurons also received synaptic conductance fluctuating noisy inputs[65,67,68]. The mean conductance of the synaptic noise was set as 20% of g_{Leak} for excitatory noise and 80% of g_{Leak} for inhibitory noise for all neurons[39]. The SD deviation of the synaptic noise was set to 100%, 60%, and 150% of the mean conductance for TC, NRT and PY neurons, respectively, in order to induce fluctuations of spike timing that reflect those observed in the experimental data. The synaptic weight of the cortico-thalamic EPSPs was adjusted to induce a spiking probability similar to that of our experimental data (Supplementary Table 3). All neurons had T-type Ca^{2+} channels and thus were able to generate rebound bursts after a hyperpolarizing pulse.

In addition to those basal conditions of the cortico-thalamic network described above, which reflect the interictal neuronal state, the two PY model neurons received identical inputs consisting of trains of 5 AMPA EPSPs (modelled as in Ref. 51). No other external input was delivered to either the TC or the NRT neurons. The inter-EPSP interval within a train was randomly drawn from a Poisson distribution with a mean of 3 ms. The inter-train interval was randomly drawn from a Poisson distribution with a mean of 140 ms, which produced an average frequency of 7 Hz, similar to the SWD frequency in GAERS. Twenty-second-long simulations were repeated 40 times with different noise seeds. Simulated firing activity was analyzed as the experimental data. Time-zero for the simulated firing distribution plots was taken as the 3rd EPSPs of a train: selecting either earlier or later EPSPs in the train had no major effects on the simulation results.

Statistical analysis

Paired Wilcoxon signed-rank test was used for the effect of TTA-P2 on TC neuron firing and ASs. Circular statistics (Kuiper test and concentration factors) was used to compare phase distributions across the SWC epoch (Fig. 7d and Supplementary fig12a,c). Kolmogorov-Smirnov test was used for spike time distribution around the SWC spike (Fig 4). Normality and equal variances were not assumed by the tests employed.

Permutations were used for non-parametric tests applied to compare experimental XCors to XCors expected if spikes would occur at times drawn randomly from their distribution around the SWC spike time (Figs. 5, 6, 8) (Supplementary Figs. 8, 10a). The same number of spike time pairs as in the experimental XCors is drawn from the respective TC, NRT and cortical neuron density distributions around the SWC-spike time. Computing their XCors allowed us to generate a surrogate XCor where spikes are shuffled independently from each other but respecting the probability distribution to find them at particular times around the SWC-spike time. Repeating the process 1000 times allowed us to estimates the 5% and 95% limits (confidence interval) for the surrogate XCor which could be directly compared to experimental XCors. This method is more stringent than simple spike-time shuffling around their measured times69, since it takes into account specific spike-times associated to an external source of synchronization which can generate peaks and troughs without any direct relationships between neurons.

Supplementary Material

Refer to Web version on PubMed Central for supplementary material.

Acknowledgments

References

1. McCormick DA, Bal T. Sleep and Arousal: Thalamocortical Mechanisms. Annu Rev Neurosci. 1997; 20:185–215. [PubMed: 9056712]

2. Crunelli V, Hughes SW. The slow (1 Hz) rhythm of non-REM sleep: a dialogue between three cardinal oscillators. Nat Neurosci. 2010; 13:9–17. [PubMed: 19966841]

3. Schmitt LI, et al. Thalamic amplification of cortical connectivity sustains attentional control. Nature. 2017; 545:219–223.

4. Steriade, M.; Jones, EG.; McCormick, DA. Thalamus - Organisation and function. Vol. 1. Elsevier Science; 1997.

5. Crunelli V, et al. Dual function of thalamic low-vigilance state oscillations: rhythm-regulation and plasticity. Nat Rev Neurosci. 2018; 19:107–118.

6. Contreras, Diego; Steriade, Mircea. Spindle oscillation in cats: the role of corticothalamic feedback in a thalamically generated rhythm. J Physiol. 1996; 490:159*79.

7. McCormick DA, Contreras D. On the cellular and network bases of epileptic seizures. Annu Rev Physiol. 2001; 63:815–46.

8. Crunelli V, Leresche N. Childhood Absence Epilepsy: Genes,Channels,Neurons and Networks. Nat Rev Neurosci. 2002; 3:371–82.

9. Blumenfeld H. Cellular and network mechanisms of spike-wave seizures. Epilepsia. 2005; 46:21–33. [PubMed: 16302873]

10. von Krosigk M, Bal T, McCormick DA. Cellular mechanisms of a synchronized oscillation in the thalamus. Science. 1993; 261:361–4.

11. Huntsman MM, Porcello D, Homanics GE, DeLorey TM, Huguenard JR. Reciprocal Inhibitory Connections and Network Synchrony in the Mammalian Thalamus. Science. 1999; 283:541–543.

12. Destexhe A. Spike-and-wave oscillations based on the properties of GABAB receptors. J Neurosci. 1998; 18:9099–9111.

13. Destexhe, A. Neuronal Networks in Brain Function, CNS Disorders, and Therapeutics. Elsevier Inc.; 2014. p. 11-35.

14. Pinault D, et al. Intracellular recordings in thalamic neurones during spontaneous spike and wave discharges in rats with absence epilepsy. J Physiol. 1998; 509:449–456.

15. Steriade M, Contreras D. Relations between cortical and thalamic cellular events during transition from sleep patterns to paroxysmal activity. J Neurosci. 1995; 15:623–642.

16. Slaght SJ, Leresche N, Deniau J-M, Crunelli V, Charpier S. Activity of thalamic reticular neurons during spontaneous genetically determined spike and wave discharges. J Neurosci. 2002; 22:2323–2334.

17. Inoue M, Duysens J, Vossen JMH, Coenen AML. Thalamic multiple-unit activity underlying spike-wave discharges in anesthetized rats. Brain Res. 1993; 612:35–40.

18. Inoue M, Ates N, Vossen JMH, Coenen AML. Effects of the neuroleptanalgesic fentanyl-fluanisone (Hypnorm) on spike-wave discharges in epileptic rats. Pharmacol Biochem Behav. 1994; 48:547–551.

19. Depaulis A, David O, Charpier S. The genetic absence epilepsy rat from Strasbourg as a model to decipher the neuronal and network mechanisms of generalized idiopathic epilepsies. J Neurosci Methods. 2015; 260:1–16.

20. Taylor H, et al. Investigating local and long-range neuronal network dynamics by simultaneous optogenetics, reverse microdialysis and silicon probe recordings in vivo. J Neurosci Methods. 2014; 235:83–91.

21. Venzi M, Di Giovanni G, Crunelli V. A critical evaluation of the gamma-hydroxybutyrate (GHB) model of absence seizures. CNS Neurosci Ther. 2015; 21:123–140.

22. Meeren HKM, Pijn JPM, Van Luijtelaar ELJM, Coenen AML, Lopes da Silva FH. Cortical focus drives widespread corticothalamic networks during spontaneous absence seizures in rats. J Neurosci. 2002; 22:1480–1495.

23. Polack P-O, et al. Deep Layer Somatosensory Cortical Neurons Initiate Spike-and-Wave Discharges in a Genetic Model of Absence Seizures. J Neurosci. 2007; 27:6590–6599.

24. Hazan L, Zugaro M, Buzsáki G. Klusters, NeuroScope, NDManager: a free software suite for neurophysiological data processing and visualization. J Neurosci Methods. 2006; 155:207–16. [PubMed: 16580733]

25. Barthó P, et al. Ongoing network state controls the length of sleep spindles via inhibitory activity. Neuron. 2014; 82:1367–1379. [PubMed: 24945776]

26. Halassa MM, et al. State-Dependent Architecture of Thalamic Reticular Subnetworks. Cell. 2014; 158:808–821.

27. Dreyfus FM, et al. Selective T-type calcium channel block in thalamic neurons reveals channel redundancy and physiological impact of I(T)window. J Neurosci. 2010; 30:99–109.

28. David F, et al. Essential Thalamic Contribution to Slow Waves of Natural Sleep. J Neurosci. 2013; 33:19599–19610.

29. Talley EM, et al. Differential distribution of three members of a gene family encoding low voltage-activated (T-type) calcium channels. J Neurosci. 1999; 19:1895–1911.

30. Kim D, et al. Lack of the burst firing of thalamocortical relay neurons and resistance to absence seizures in mice lacking alpha(1G) T-type Ca(2+) channels. Neuron. 2001; 31:35–45.

31. Ernst WL, Zhang Y, Yoo JW, Ernst SJ, Noebels JL. Genetic enhancement of thalamocortical network activity by elevating alpha 1g-mediated low-voltage-activated calcium current induces pure absence epilepsy. J Neurosci. 2009; 29:1615–25.

32. Buzsáki G. The thalamic clock: emergent network properties. Neuroscience. 1991; 41:351–64.

33. Sorokin JM, et al. Bidirectional Control of Generalized Epilepsy Networks via Rapid Real-Time Switching of Firing Mode. Neuron. 2017; 93:194–210.

34. Cope DW, et al. Enhanced tonic GABAA inhibition in typical absence epilepsy. Nat Med. 2009; 15:1392–8.

35. Connelly WM, et al. GABAB Receptors Regulate Extrasynaptic GABAA Receptors. J Neurosci. 2013; 33:3780–5.

36. Herd MB, Brown AR, Lambert JJ, Belelli D. Extrasynaptic GABA(A) receptors couple presynaptic activity to postsynaptic inhibition in the somatosensory thalamus. J Neurosci. 2013; 33:14850–14868.

37. Cope DW. GABAA Receptor-Mediated Tonic Inhibition in Thalamic Neurons. J Neurosci. 2005; 25:11553–11563.

38. Crandall SR, Cruikshank SJ, Connors BW. A Corticothalamic Switch: Controlling the Thalamus with Dynamic Synapses. Neuron. 2015; 86:768–782.

39. Deleuze C, et al. T-Type Calcium Channels Consolidate Tonic Action Potential Output of Thalamic Neurons to Neocortex. J Neurosci. 2012; 32:12228–12236.

40. Powell KL, et al. A Cav3.2 T-type calcium channel point mutation has splice-variant-specific effects on function and segregates with seizure expression in a polygenic rat model of absence epilepsy. J Neurosci. 2009; 29:371–380.

41. Chen Y, et al. Association between genetic variation of CACNA1H and childhood absence epilepsy. Ann Neurol. 2003; 54:239–243.

42. Lee SE, et al. Rebound burst firing in the reticular thalamus is not essential for pharmacological absence seizures in mice. Proc Natl Acad Sci U S A. 2014; 111:1–6.

43. Gentet LJ, Ulrich D. Strong, reliable and precise synaptic connections between thalamic relay cells and neurones of the nucleus reticularis in juvenile rats. J Physiol. 2003; 546:801–811.

44. Kim U, McCormick DA. The functional influence of burst and tonic firing mode on synaptic interactions in the thalamus. J Neurophysiol. 1998; 18:9500–9516.

45. Cruikshank SJ, Urabe H, Nurmikko AV, Connors BW. Pathway-Specific Feedforward Circuits between Thalamus and Neocortex Revealed by Selective Optical Stimulation of Axons. Neuron. 2010; 65:230–245.

46. Mease RA, Krieger P, Groh A. Cortical control of adaptation and sensory relay mode in the thalamus. Proc Natl Acad Sci U S A. 2014; 111:6798–803.

47. Maheshwari A, Noebels JL. Progr Brain Res. 2014; 213:223–252.

48. Paz JT, et al. A new mode of corticothalamic transmission revealed in the Gria4(-/-) model of absence epilepsy. Nat Neurosci. 2011; 14:1167–73.

49. Mangan KP, et al. Tonic Inhibition is Abolished in GABAA Receptor γ2R43Q Knock-in Mice with Absence Epilepsy and Febrile Seizures. bioRxiv. 2017 155556.

50. Guo JN, et al. Impaired consciousness in patients with absence seizures investigated by functional MRI, EEG, and behavioural measures: a cross-sectional study. Lancet Neurol. 2016; 15:1336–1345.

51. Lidster K, et al. Opportunities for improving animal welfare in rodent models of epilepsy and seizures. J Neurosci Methods. 2015; 260:2–25.

52. Paxinos, G.; Watson, C. The Rat Brain in Stereotaxic Coordinates. 6th Edition. Academic Press Inc; 2007.

53. Vandecasteele M, et al. Large-scale recording of neurons by movable silicon probes in behaving rodents. J Vis Exp. 2012:e3568.

54. Harris KD, Henze D, Csicsvari J. Accuracy of tetrode spike separation as determined by simultaneous intracellular and extracellular measurements. J Neurophysiol. 2000; 84:401–414.

55. Celeux G, Govaert G. A classification EM algorithm for clustering and two stochastic versions. Comput Stat Data Anal. 1992; 14:315–332.

56. Henze, Da, et al. Intracellular features predicted by extracellular recordings in the hippocampus in vivo. J Neurophysiol. 2000; 84:390–400.

57. Pedreira C, Martinez J, Ison MJ, Quian Quiroga R. How many neurons can we see with current spike sorting algorithms? J Neurosci Methods. 2012; 211:58–65.

58. Pouzat C. Improved Spike-Sorting By Modeling Firing Statistics and Burst-Dependent Spike Amplitude Attenuation: A Markov Chain Monte Carlo Approach. J Neurophysiol. 2004; 91:2910–2928.

59. Schmitzer-Torbert N, Jackson J, Henze D, Harris K, Redish AD. Quantitative measures of cluster quality for use in extracellular recordings. Neuroscience. 2005; 131:1–11.

60. Domich L, Oakson G, Steriade M. Thalamic Burst Patterns in the Naturally Sleeping Cat: a Comparison Between Cortically Projecting and Reticularis Neurones. J Physiol. 1986; 379:429–449.

61. Steriade M, Domich L, Oakson G. Reticularis thalami neurons revisited: activity changes during shifts in states of vigilance. J Neurosci. 1986; 6:68–81.

62. Barthó PP, et al. Characterization of Neocortical Principal Cells and Interneurons by Network Interactions and Extracellular Features. J Neurophysiol. 2004; 92:600–608.

63. Vinck M, Battaglia FP, Womelsdorf T, Pennartz C. Improved measures of phase-coupling between spikes and the Local Field Potential. J Comput Neurosci. 2012; 33:53–75.

64. Hines ML, Carnevale NT. NEURON: a tool for neuroscientists. Neuroscientist. 2001; 7:123–135.

65. Destexhe, a; Bal, T.; McCormick, Da; Sejnowski, TJ.; Destexhe, TJ. Ionic mechanisms underlying synchronized oscillations and propagating waves. J Neurophys. 1996; 76:2049–2070.

66. Destexhe A, Contreras D, Steriade M. LTS cells in cerebral cortex and their role in generating spike-and-wave oscillations. Neurocomputing. 2001; 38:555–563.

67. Wolfart J, Debay D, Le Masson G, Destexhe A, Bal T. Synaptic background activity controls spike transfer from thalamus to cortex. Nat Neurosci. 2005; 8:1760–1767.

68. Destexhe A, Mainen ZF, Sejnowski TJ. Synthesis of models for excitable membranes, synaptic transmission and neuromodulation using a common kinetic formalism. J Comput Neurosci. 1994; 1:195–230.

69. Fujisawa S, Amarasingham A, Harrison MT, Buzsáki G. Behavior-dependent short-term assembly dynamics in the medial prefrontal cortex. Nat Neurosci. 2008; 11:823–833.
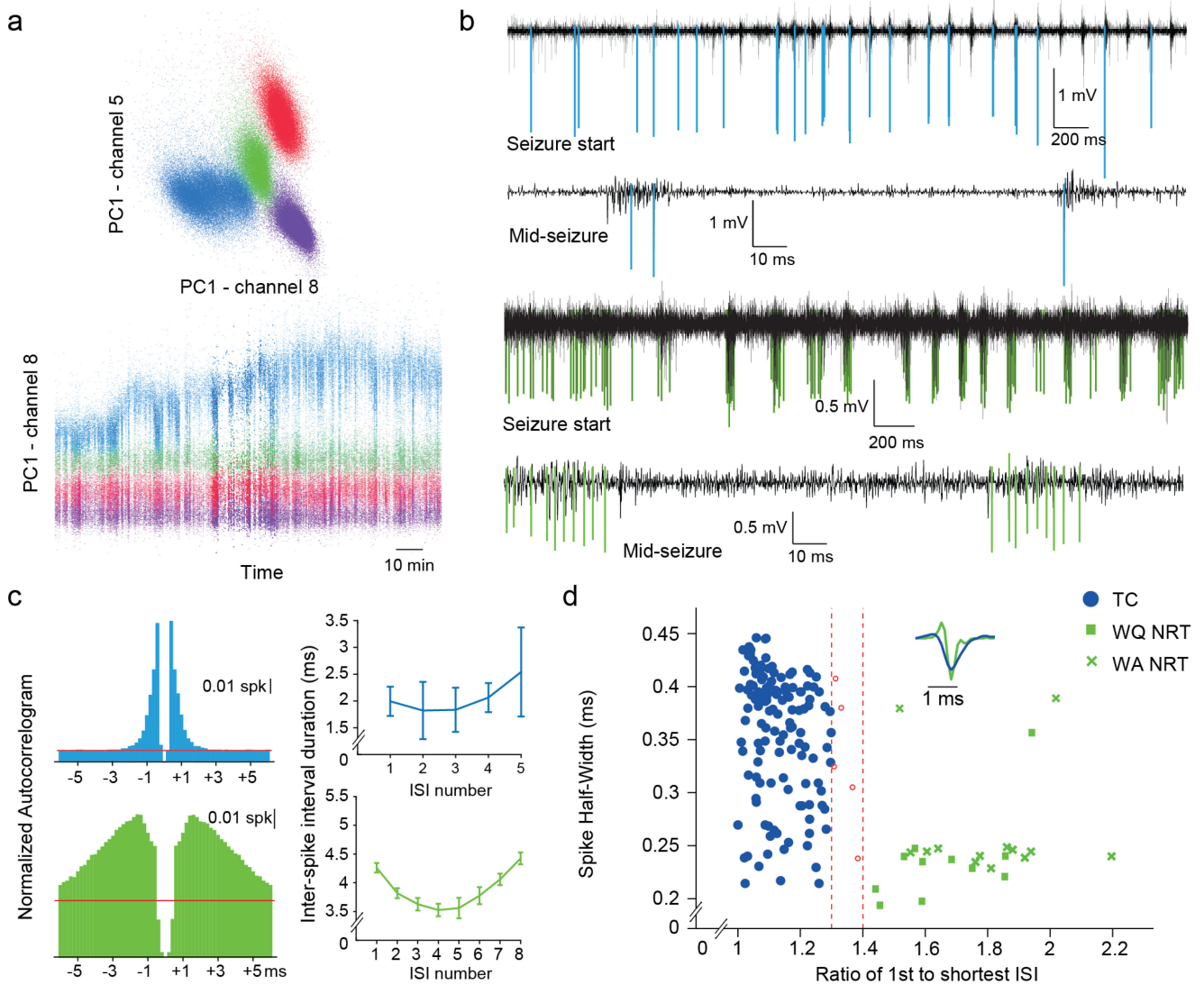
Figure 1. Spike clustering and thalamic neuronal type identification.
(**a**) Automated spike sorting by clustering of principal components (PC) in multiple dimensions, reflecting spike amplitude and spike shape. (**b**) High-pass filtered traces showing typical isolated action potentials of TC (blue, top two traces) and NRT (green, bottom two traces) neurons spikes at start and middle of ASs. (**c**) Autocorrelograms (left) and plots of mean interspike interval (ISI) versus interspike number of high frequency bursts (right) for a TC (blue) and an NRT neuron (green) during ASs. Error bars indicate ±SEM. Note the clear NRT neuron accelerando-decelerando pattern. (**d**) Spike half-width vs. burst acceleration index (ratio of 1st to shortest ISI in a burst) for all neurons. Red dashed lines indicate acceleration index <1.3 for TC (n=139) and >1.4 for NRT (n=25) neurons used to identify the two neuron types (Online Methods). Neurons marked in red were excluded from further analysis. Inset depicts superimposed typical TC (blue) and NRT (green) spike waveforms.
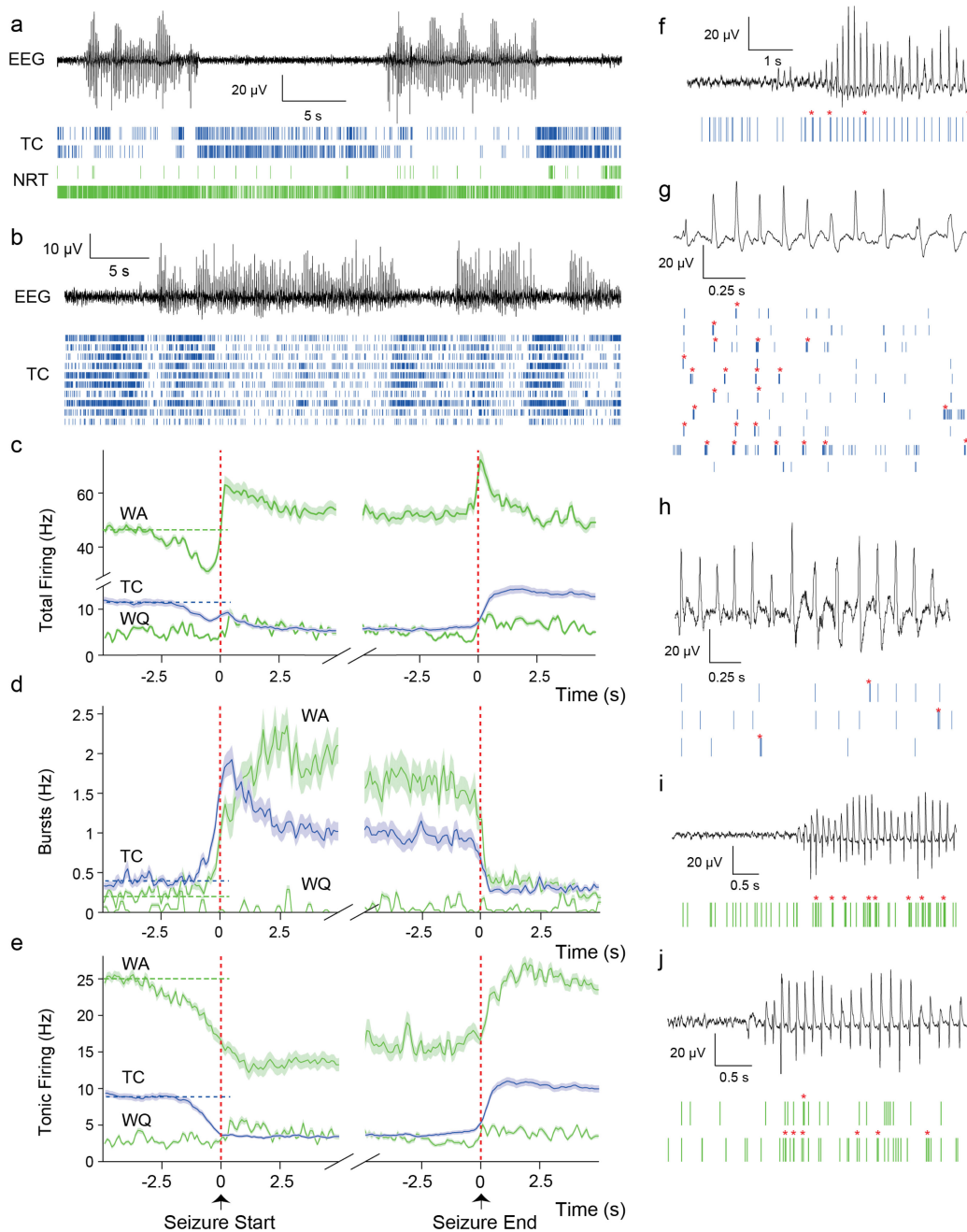
Figure 2. Temporal dynamics of TC and NRT neuron ensemble firing during ASs in GAERS.
(**a**) Spike-time raster plots (bottom traces) from 2 TC (blue) and 2 NRT (green, top wake-quiescent, bottom wake-active) neurons with time-matched EEG (top trace) in a GAERS. Note the sparse firing of TC neurons during ASs and the diverse firing of the two NRT neurons. (**b**) Spike-time raster plots (bottom traces) from 10 TC neurons with time-matched EEG (top trace) in another GAERS. Note the decrease in TC neuron firing during ASs. (**c**,**d**,**e**) Temporal evolution of total (**c**), burst (**d**) and tonic (**e**) firing before, during and after ASs for TC (blue) and NRT neurons (green) (lines: mean, shaded areas: ±SEM) (n=1216

SWDs; n=139 TC neurons; n=13 wake-active, WA, and 12 wake-quiescent, WQ, NRT neurons). Note the similar rate of increase (1.2 Hz/s) of bursts in TC and NRT neurons from about 1 s before SWD detection in the EEG. At the time of the peak of burst firing of TC neurons, NRT bursts continue to increase but at a slower rate (0.5 Hz/s). Vertical red dashed lines indicate the start and end of SWDs in the EEG; horizontal dashed lines indicate mean pre-ictal firing rates. (**f-j**) Spike-time raster plots (bottom traces) and time-matched EEG (top trace) for different TC and NRT neurons at interictal-to-ictal transitions (**f,i,j**), at the very start of an AS (**g**) and in the middle of an AS (**h**). Note the high prevalence of bursts (red asterisks) in TC and NRT neurons at the start of ASs.
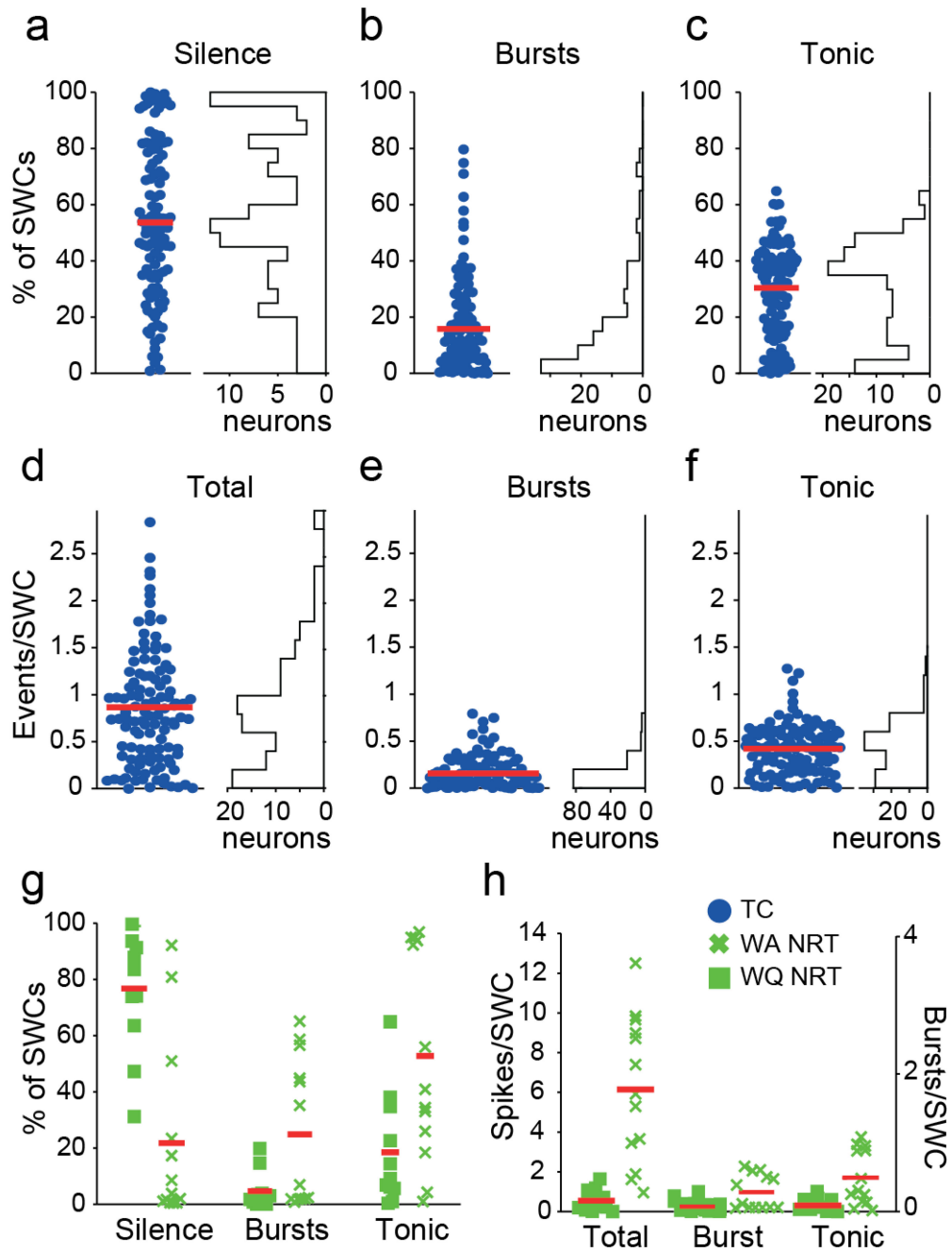
Figure 3. Ictal firing properties during ASs in GAERS.
(**a**,**b**,**c**) Electrical silence (**a**), bursts (**b**) and tonic (**c**) firing observed at each SWCs are plotted as percentage of SWCs for each TC neuron (left) and as distribution for the TC neuron population (right) (n=139). Twelve (9%) TC neurons were completely silent during ASs and 62 (45%) were silent for >50% of SWCs. Moreover, 33 (24%) TC neurons showed no burst during ASs, 84 (61%) neurons exhibited bursts for <20% of SWCs and no TC neuron had bursts for >80% of SWCs. (**d**,**e**,**f**) Number of events per SWC for total (**d**), bursts (**e**) and tonic firing (**f**) are plotted for each TC neuron (left) and as a distributions for

the TC neuron population (right) (n=139 neurons). (**g**) Same plots as in **a-c** for WA and WQ NRT neurons. (**h**) Same plots as in **d-e** for WA and WQ NRT neurons. Red lines in **a-h** indicate mean values.
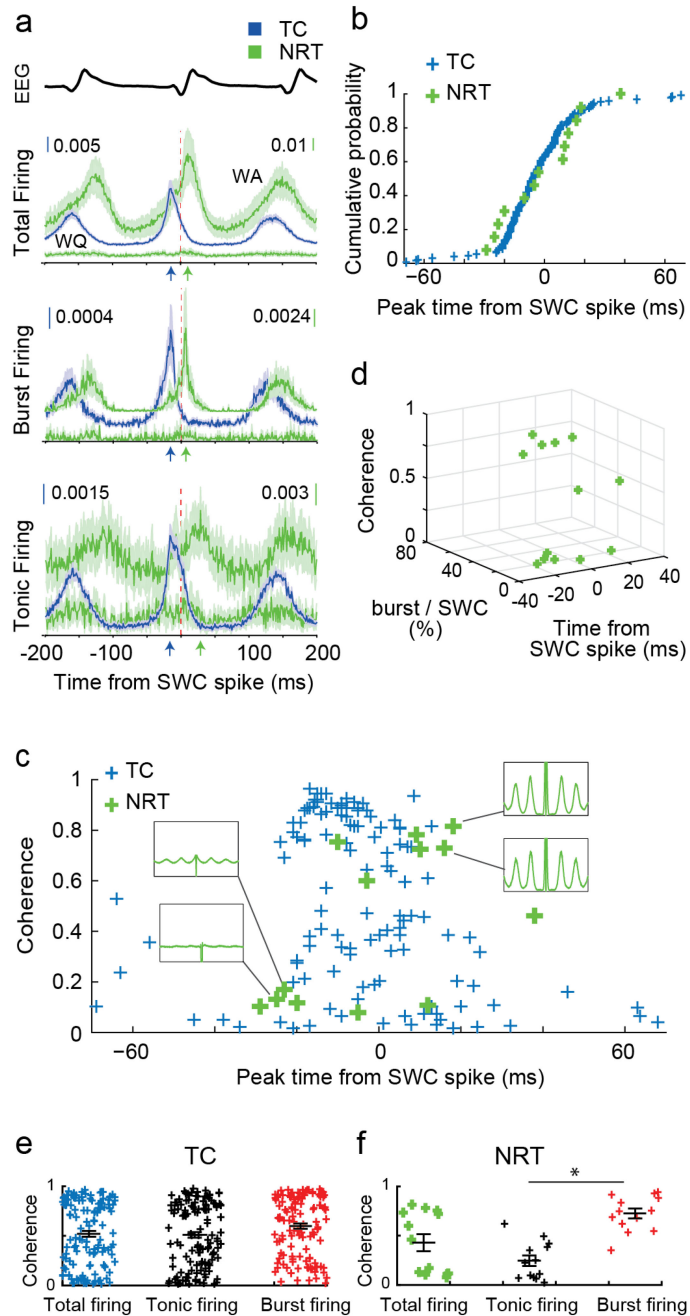
Figure 4. Synchrony and coherence of TC and NRT neuron firing during ASs.
(**a**) SWC-spike-triggered averages (lines: mean; shaded areas: ±SEM) of total, burst and tonic firing for GAERS TC (n=139 in all subfigures), WA (n=13 in all subfigures) and WQ (n=12) NRT neurons. Note the different peak times (color-coded arrows) of TC and NRT neurons relative to SWC spike (red vertical line). (**b**) Cumulative probability distributions of peak time of total firing for individual TC (blue) and WA NRT (green) neurons show no statistical difference between the two neuronal populations (p=0.631; Kolmogorov-Smirnov test). (**c**) SWC coherence of total firing vs peak time of total firing for individual GAERS

TC and WA NRT neurons. Note the high coherence for TC neurons with peak firing times between -20 to 0 ms. In contrast, NRT neurons show low coherence (and flat autocorrelograms, left green insets) when their firing peaks occur in the -20 to 0 ms interval but high coherence (and clear peaks in the autocorrelograms, right green insets) when their firing peaks is after 0 ms. (**d**) 3D-plot showing NRT neurons with high coherence have a relatively high burst rate and fire relatively late with respect to the SWC-spike, while those NRT neurons with low coherence have a relatively low burst rate and fire early with respect to the SWC spike. (**e**) SWC coherence for different firing types (mean ± SEM in black) for individual TC (**e**) and NRT (**f**) neurons. Note the higher coherence of burst vs tonic firing in NRT neurons (*p=7×10^{-5}, n=13 neurons, two-sided signed rank test).
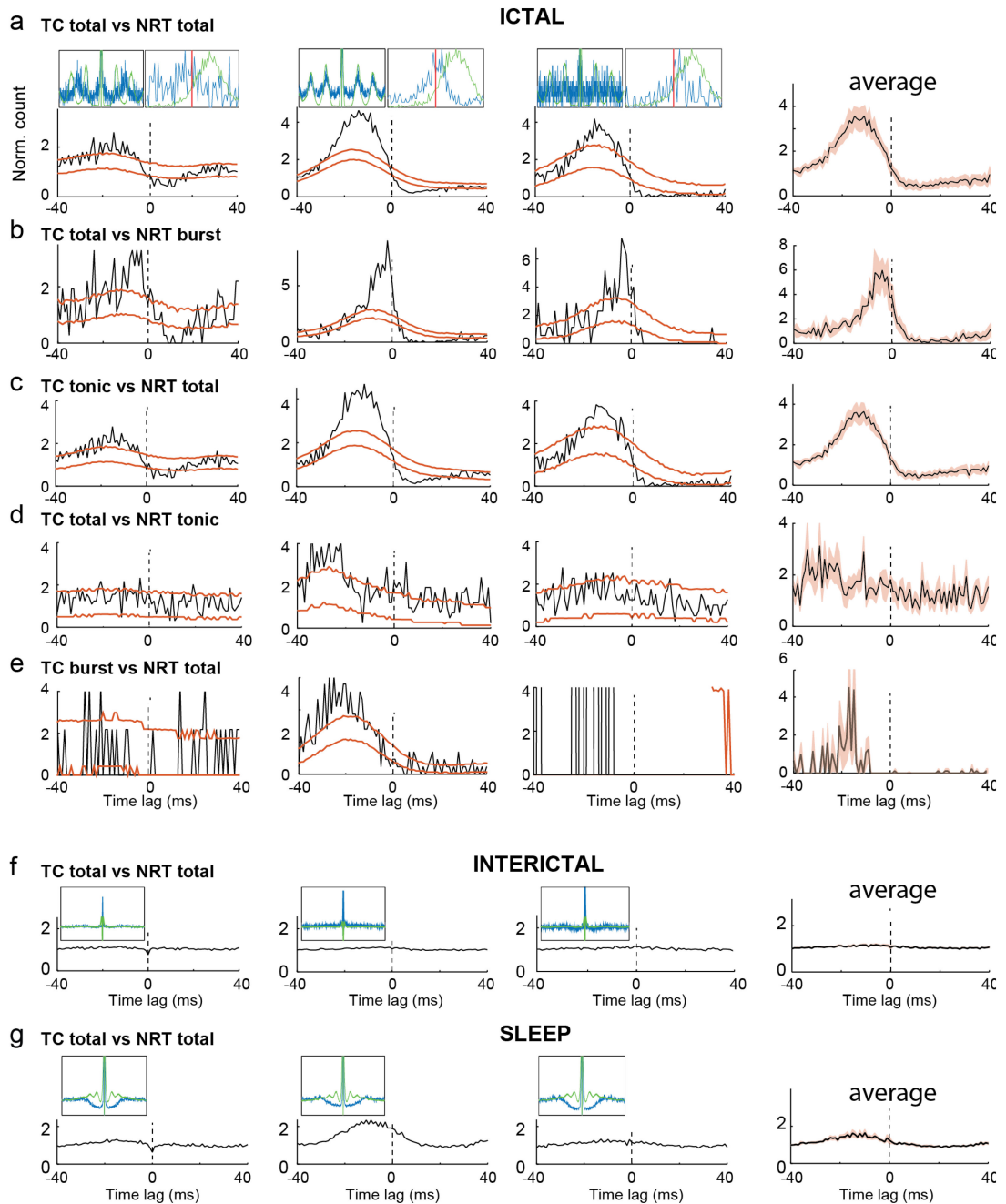
Figure 5. Ictal recruitment of NRT-TC neuron inhibitory assemblies.
(**a-g**) Representative crosscorrelograms (XCors) (black trace) of firing of three
representative pairs of simultaneously recorded TC and NRT neurons (3 leftmost columns)
(orange lines indicate expected confidence intervals (5-95%) estimated from surrogate firing
time trains for each neuron in its respective firing distribution relative to the SWC)
(Supplementary Methods). The average XCors (black line; red shadow: ± SEM) of 5 pairs is
shown in the rightmost column. The significant (below CI) troughs after 0 ms in the XCors
indicates a lower probability of the TC neuron to fire after an NRT spike (**a**), and is

maintained when NRT burst firing (**b**) or TC tonic firing (**c**) are used for the analysis. No statistically significant sharp peak or trough is present when NRT tonic firing (**d**) or TC burst firing (**e**) are used. The same 3 pairs do not exhibit these peaks or troughs during interictal periods (**f**) and non-REM sleep (**g**). Top left insets in (**a**,**f**,**g**) show superimposed autocorrelograms for the respective TC (blue) and NRT (green) neurons calculated between -400 and +400 ms from the SWC-spike. Top right insets in (**a**) show superimposed spike distribution of the respective TC (blue) and NRT (green) neuron calculated from -40 to +40 ms of the SWC-spike (red lines). For both insets, each curve maximum amplitude is normalized to 1.
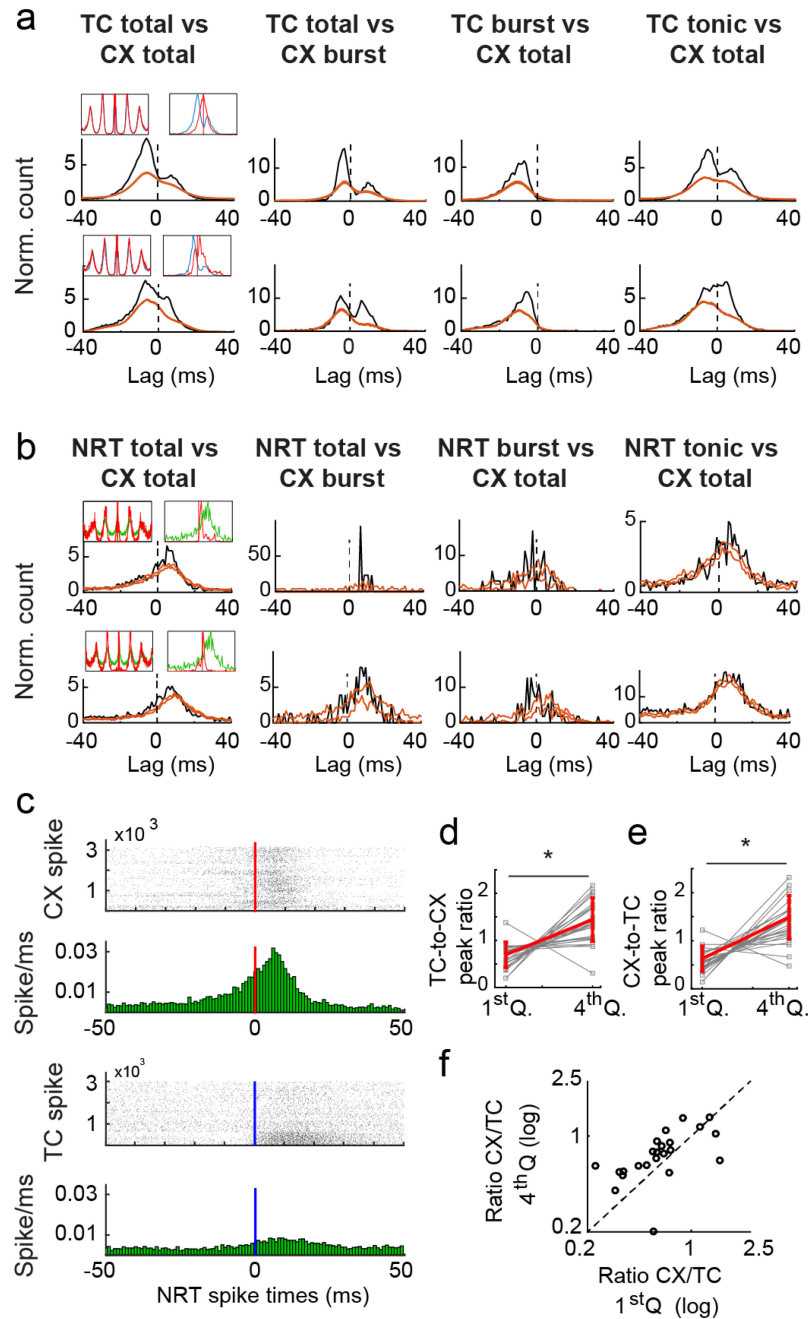
Figure 6. Ictal cortical drive of thalamic neuronal populations.
(**a**) Representative crosscorrelograms (XCors) (black trace) of firing of two representative pairs of simultaneously recorded TC and cortical (CX) neurons (orange lines indicate expected confidence intervals (5-95%) estimated as described in Fig. 5). The presence of two peaks, one before and one after time-zero, which are more evident when only CX neuron bursts were used for the analysis, indicates reciprocal excitation between TC and CX neurons. Top left insets show superimposed autocorrelograms for the respective TC (blue) and CX (red) neurons calculated between -400 and +400 ms from the SWC spike. Top right

insets show superimposed spike distribution of the respective TC (blue) and CX (red) neuron calculated from -40 to +40 ms with respect to the SWC-spike (red lines). For both insets, each curve maximum amplitude is normalized to 1. (**b**) Representative XCors as in (**a**) but for two representative pairs of simultaneously recorded NRT and CX neurons. The significant peak after time zero indicates the increased probability of NRT neuron firing following CX firing. Note how this peak is much larger and sharper when only CX burst firing is used for the analysis. Top left and right insets in (**b**) are as in (**a**) but for NRT (green) and CX (red) neurons. (**c**) Peri-spike raster plots (top graphs) and histograms (bottom graphs) of NRT firing with respect to CX and TC neuron spike occurring at time 0 (red and blue line, respectively), calculated from simultaneously recorded CX-NRT and TC-NRT pairs. In the histograms, note the clear peak (6th bin after time-zero) following CX but not TC neuron firing (horizontal red and blue line, respectively). (**d**) Ratio of the XCors peaks of TC-to-CX interaction (i.e. peak before time-zero) for the 1st and 4th quartiles of SWC-spike amplitudes over peaks for all SWC-spike amplitudes (Supplementary Figure 10b) (Supplementary Methods) (*$p=1.26 \times 10^{-4}$, one-sided signed rank test, n=25 independent pairs of TC-CX neurons). (**e**) Same plot as (**d**) for the XCors peak of CX-to-TC interactions (i.e. peak after time-zero) (*$p=3.04 \times 10^{-5}$, one-sided signed rank test, n=25 pairs of neurons). (**f**) Ratio of CX-TC and TC-CX peaks for the highest versus the lowest SWC-spike amplitude quartile indicate a gain of cortico-thalamic over the thalamo-cortical contribution to the XCors ($p=8.3 \times 10^{-3}$, one-sided signed rank test, n=25 neuron pairs) for the largest SWC-spike.
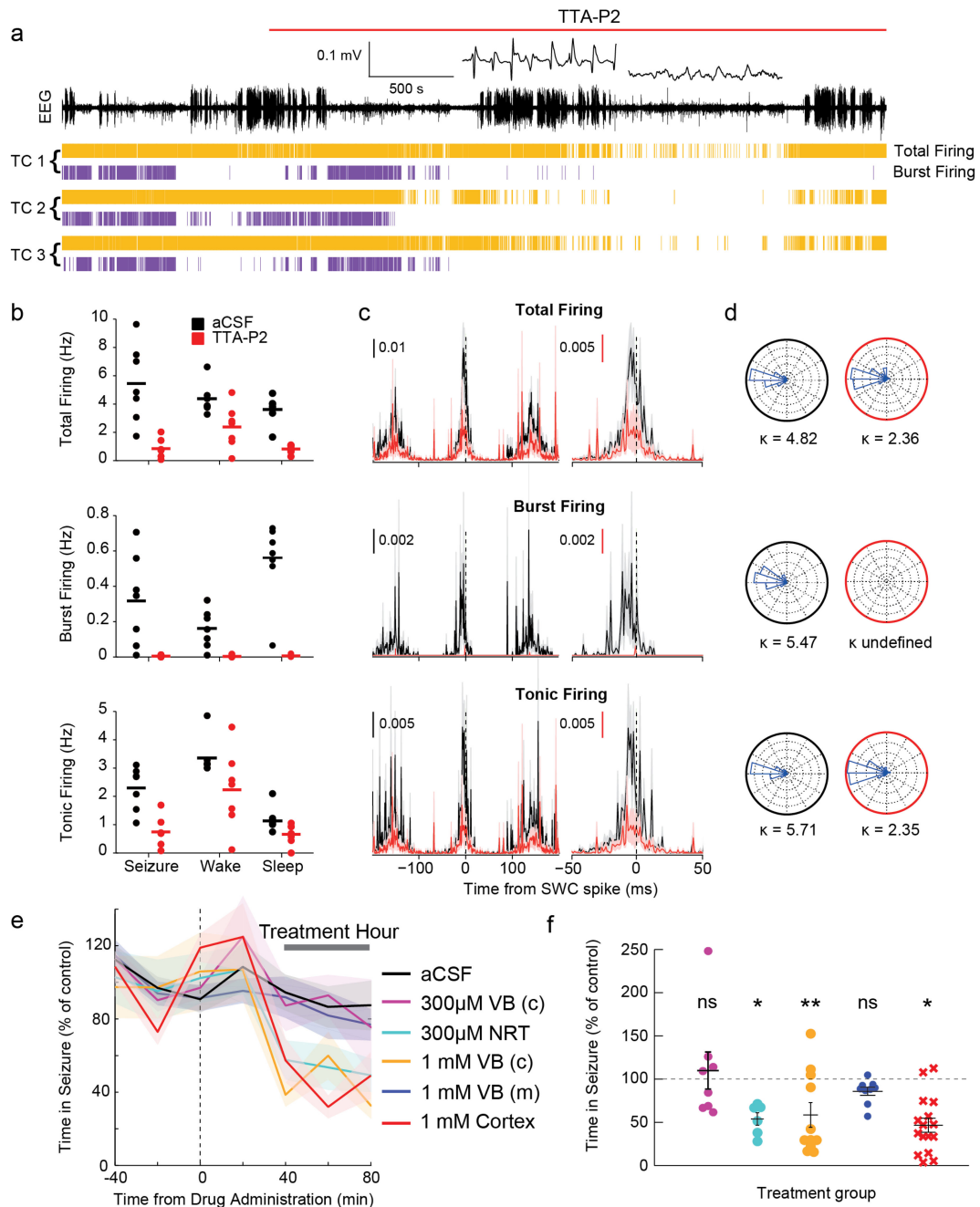
Figure 7. Block of T-channels in NRT and S1pO cortex markedly reduces ASs whereas block in TC neurons does not affect thalamic output synchrony or behavioural ASs.
(**a**) EEG (top trace), and spike-time (yellow) and burst-time (violet) raster plots (bottom traces) from 3 simultaneously recorded TC neurons in GAERS VB before and during reverse microdialysis administration of 300μM TTA-P2 (marked by red line) from an adjacent microdialysis probe. Note the complete block of bursts by TTA-P2 during both ASs and sleep periods (enlarged left and right trace, respectively, at the top of the EEG record). (**b**) Rates of different firing types before (black) and during (red) complete block of bursts by TTA-P2 show decrease in total (p=0.014), burst (p=0.015), and tonic (p=0.031) firing

during ASs, and in total (p=0.031) and burst (p=0.015) but not tonic (p=0.16) firing during wakefulness (paired two-sided Wilcoxon signed-rank test). Horizontal lines indicate the mean of n=7 TC neurons. (**c**) SWC-triggered means of different firing types (total, burst, tonic) of n=7 TC neurons show clear peaks near the EEG SWC spike (indicated by the vertical black dashed line) before (black) and during (red) complete block of bursts by TTA-P2. Error bars (shaded areas) indicate ±SEM. (**d**) Circular firing distribution and circular concentration coefficient (κ) showing similar value before (black circles) and during TTA-P2 (red circles) administration (n=7 independent neurons, Kuiper test, p=0.024; κ undefined for burst firing during TTA-P2 dialysis since bursts were completely abolished). (**e**) Time-course of total time in seizure before and during bilateral thalamic reverse microdialysis of aCSF or different concentrations of TTA-P2 in GAERS (lines and shaded areas: mean ± SEM; Treatment Hour indicates the period analysed in (**f**). Black dashed vertical line indicates the start of TTA-P2 dialysis. n=8 GAERS with 300µM TTA-P2 in the centre of the VB (VB(c)), 11 with 1mM TTA-P2 in VB(c), 6 with 300µM in NRT, 9 with TTA-P2 medially to the centre of the VB (VB(m)) and 16 with 1 mM TTA-P2 in S1pO cortex. Note that microdialysis of 1mM TTA-P2 in VB(c) blocks bursts both in VB and NRT28. (**f**) Mean total time spent in seizure by GAERS during different TTA-P2 applications (n as in (**e**)) was calculated during the treatment hour as percentage of the control hour (prior to TTA-P2 administration) (color-code as in **e**; black horizontal lines: mean (±SEM), p=0.7422, 0.0313, 0.0186, 0.7344, 0.0182, paired two-sided Wilcoxon signed-rank test). The effect of TTA-P2 on number and duration of ASs, and on SWD frequency is illustrated in Supplementary Fig. 12.
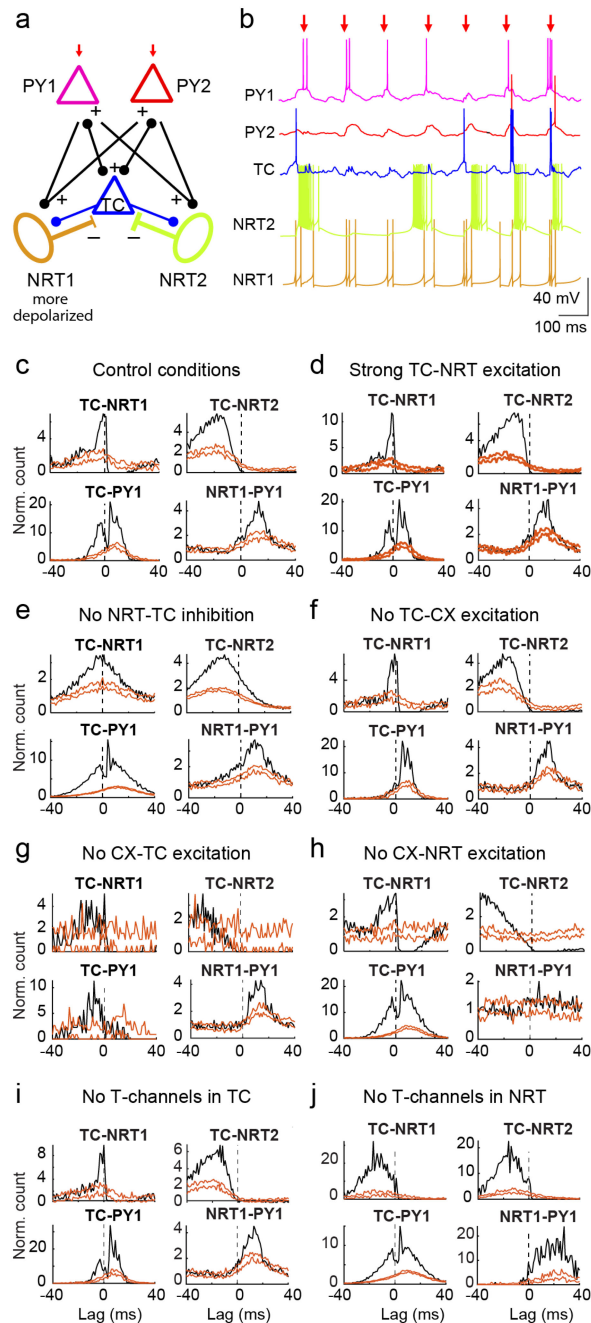
Figure 8. Firing interactions in a cortico-thalamic network model.
(**a**) Schematic diagram of the model network, consisting of 1 TC, 2 NRT and 2 excitatory cortical pyramidal neurons (PY). NRT1 is more depolarized than NRT2 via steady injected current. Excitatory (AMPA) synapses connect TC to NRT and PY neurons, and PY neurons to NRT and TC neurons. Inhibitory GABAA synapses connect NRT to TC neurons. Only PY neurons receive a train of 5 AMPA EPSPs that is repeated at a frequency of 7 Hz (red arrows indicate the 3rd EPSP in the train which was used as time-reference for the analysis). (**b**) Example membrane potential traces illustrate the firing dynamics during 7 Hz

stimulation protocol. Note the presence of high frequency bursts in NRT2 and their paucity in TC and NRT1 neuron. **(c-j)** XCors (black) of simulated firing of different neuron pairs under various conditions (orange lines indicate expected confidence intervals (5-95%) estimated as in Fig. 5 using the 3rd EPSPs as time-reference). The simulation under "control" conditions well reproduced the experimental XCors (**c**), and no major change was observed in simulations with an increase in the strength of the TC-to-NRT neuron synapse up to 6-fold that of the CX-NRT neuron synapses (**d**), whereas blocking the NRT-to-TC neuron GABAA synapses abolished the trough after time zero in TC-NRT neuron XCors (**e**). Block of cortical to TC neuron synapses or vice versa led to TC-CX XCors that were different from those observed experimentally (**f, g**), and while a trough was still present in TC-NRT XCors when the cortical input to NRT neurons was absent, there was no peak in NRT-CX XCors (**h**). Removal of T-channels in TC neurons had no major effect on the XCors (**i**), whereas in NRT neurons led to broader XCors peaks (**j**) compared to the control conditions (**a**).